The Dynamics of the Antarctic Circumpolar Current

VLADIMIR O. IVCHENKO AND KELVIN J. RICHARDS

Department of Oceanography, University of Southampton, Southampton, England

DAVID P. STEVENS

School of Mathematics, University of East Anglia, Norwich, England

(Manuscript received 6 June 1994, in final form 25 September 1995)

ABSTRACT

The dynamics of the Antarctic Circumpolar Current (ACC) in a near-eddy-resolving model of the Southern Ocean (FRAM) are investigated. A streamwise coordinate system is used, rather than a more conventional approach of considering zonally averaged quantities. The motivation for this approach is the large deviation from a purely zonal flow made by the current. Comparisons are made with a zonal-mean analysis of the same model. It is found that the topographic form drag is the main sink of the momentum that is input by the wind. However, in contrast to a zonal-mean analysis other terms, namely, horizontal mixing, bottom friction, and advection of momentum, are no longer negligible. The total effect of transient eddies is to produce a drag on the mean flow, again in contrast to the zonally averaged case.

The vertical penetration of stress is considered. A generalized formula is derived for the interfacial form stress averaged along a convoluted path and that includes nonquasigeostrophic effects. The interfacial form stress is found to be related not only to the local wind stress but also to changes in stratification and the Coriolis parameter along the path of integration. The vertical gradient of the extra terms is found to be proportional to the quasi-meridional velocity averaged along an isopycnic surface. Using the model data, the nonquasigeostrophic effects are found to be important, particularly toward the northern flank of the ACC. Relating the vertical shear of the flow to the interfacial form stress, it is shown that the vertical structure of the flow is set by a combination of the wind stress and the meridional overturning. There is, therefore, an intimate linking of the wind and thermohaline-driven circulations.

1. Introduction

The Antarctic Circumpolar Current (ACC) is the strongest current in the World Ocean. The transport of the ACC in the Drake Passage as estimated from the ISOS dataset is about 130 Sv (Sv $\equiv 10^6$ m^3 s^{-1}) (Nowlin and Klinck 1986). In a number of numerical models this transport is 50–70 Sv larger (Semtner and Chervin 1988; The FRAM Group 1991). At the latitudes of the Drake Passage there are no barriers to zonal flow (in the upper ocean). It is generally thought that the wind stress is the main source of zonal momentum for the current, although thermohaline processes may also be important in driving the ACC (Olbers and Wübber 1991).

The dynamics of the ACC are complex and strongly depend upon interactions between mesoscale (synoptic) eddies, topography, and the mean flow (Gouretski et al. 1987; Wolff et al. 1990, 1991). Early models of the ACC balanced the wind stress by friction or lateral Reynolds stresses (Hidaka and Tsuchiya 1953; Gill 1968). However, a reasonable value for the ACC transport can only be obtained with unrealistically high viscosity coefficients, unrealistically large bottom friction, or high values of Reynolds stresses. Munk and Palmén (1951) were the first to describe the now generally accepted view that topographic form stress balances the wind stress. That is, the flow can establish a pressure difference across meridional ridges, with the high pressure on the western side of the ridge. Krupitsky and Cane (1994), using a simple physical model, have shown that zonal flow is strongly affected by topographic form stress. A necessary ingredient of the flow is the presence of mesoscale eddies that transfer the surface stress to the bottom where it is dissipated by the topographic form stress. A series of numerical channel model experiments have confirmed this balance (McWilliams et al. 1978; McWilliams and Chow 1981; Treguier and McWilliams 1990; Wolff et al. 1991). The same balance also occurs in the Fine Resolution Antarctic Model (FRAM), a primitive equation model of the Southern Ocean, for zonally averaged values at Drake Passage latitudes (Stevens and Ivchenko 1996). We shall call this region of the flow bounded by the southernmost and northernmost latitudes of the Drake Passage the ACC belt (ACCB).

Corresponding author address: Dr. Vladimir O. Ivchenko, Department of Oceanography, University of Southampton, Southampton S0171BJ, England.

Eddies transfer the zonal momentum downward through the action of interfacial form stress (McWilliams et al. 1978; Rhines and Holland 1979; Johnson and Bryden 1989; Marshall et al. 1993; Stevens and Ivchenko 1996). Johnson and Bryden (1989) have shown that the interfacial form stress is proportional to the meridional eddy density (heat) flux. They suggest that the interfacial form stress is established by the wind stress and does not vary with the depth. Stevens and Ivchenko (1996) generalized this formula for a zonal channel with open north and south boundaries when quasigeostrophic scaling is acceptable within the channel. In this case they show that the interfacial form stress varies as a function of depth only, $C(z)$. A clear physical interpretation for the function $C(z)$ can be understood in terms of the Eliassen–Palm fluxes (Eliassen and Palm 1961; Andrews and McIntyre 1976; Edmon et al. 1980). The function $C(z)$ is proportional to the streamfunction of the so-called residual meridional circulation.

Killworth and Nanneh (1994) examined the momentum budget on isopycnic surfaces but again along lines of constant latitude. Following a latitude line, about 40%–60% of density layers outcrop and are thus driven directly by wind. This is in contrast to quasigeostrophic theories. The main momentum balance within a density layer is the form drag on top of the layer almost equaling that at the bottom of the layer. However, the form drag is not constant with the depth but increases roughly linearly as density increases. Wells and de Cuevas (1995) have shown that the bottom pressure torque plays a dominant role in the vorticity budget of the ACC.

Many questions that have been answered for zonal channel flows or the ACCB are still open for the ACC itself. It is well known that there are strong meridional displacements of the time-mean streamlines (Gouretski et al. 1987). This is highlighted by the fact that the total time-averaged transport at the Drake Passage in FRAM is more than twice as large as the time and zonally averaged transport of the ACCB. Zonal averaging misses a large part of the flow. As we shall show in this paper, the dynamics of the zonally averaged flow is incomplete. For example, Ivchenko et al. (1996), using output from the FRAM, have found that 80% the eddy kinetic energy of the ACC is generated on the northern flank of the current, outside the ACCB. It is therefore necessary to take averages along time-mean streamlines rather than zonal averaging (Marshall et al. 1993). Here we choose to study the momentum balance of the ACC in a region following the path of the ACC, which we shall call the ACCP. The numerical results are obtained by integrating along the time-mean barotropic streamline of a primitive equation model of the Southern Ocean.

Several questions need to be answered for the ACCP. For instance:

- What are the distributions of the momentum, kinetic energy, Reynolds stresses, and density fluxes in the ACCP?
- What is the momentum balance in the ACCP, and how different is it from the ACCB?
- What kind of expression for the quasi-zonal momentum penetration is applicable for the ACCP? How different is this expression from the Johnson and Bryden (1989) formula?
- How important are nonquasigeostrophic effects and nonconstant values of the Coriolis parameter along the ACCP for the dynamics and momentum penetration?

In the rest of the paper we address these questions. In section 2, we present the distributions of momentum and kinetic energy averaged along the path of the ACC. The momentum balance along the same path from an analysis of the results of FRAM (The FRAM Group 1991) is given in section 3. In section 4 we derive a generalized expression for the vertical penetration of momentum along a convoluted path and present numerical results, again using the FRAM dataset. The paper closes with a discussion and statement of the conclusions in section 5.

2. The distribution of momentum and kinetic energy in streamline coordinates

To investigate the dynamics of the ACC we will use results from the FRAM (The FRAM Group 1991). Briefly, the model was based on the primitive equation model of Cox (1984) run at near-eddy resolution. The model domain stretched from 24°S to the Antarctic continent with a horizontal resolution of 0.5° in longitude and 0.25° in latitude. There were 32 levels in the vertical with spacing varying from 20 to 230 m. The model was spun up to the Levitus (1982) temperature and salinity fields, forced with Hellerman and Rosenstein (1983) surface stresses, and run for 16 years. The resultant flow field has many of the characteristics of the ACC. The total transport through Drake Passage, at 185 Sv, is somewhat higher than observations. The distribution of eddy energy is similar to observations but with a magnitude that is a little low. For more detailed information see Webb et al. (1991), The FRAM Group (1991), and Stevens and Killworth (1992). For our purpose the model provides a useful, dynamically consistent, dataset to which we can apply the analysis techniques developed here. We have used the velocity, temperature, and salinity fields from the last 6 years of the model run.

The 6-year averaged barotropic streamfunction is shown in Fig. 1. As can be seen, the ACC follows a convoluted path. Individual streamlines undergo large changes in latitude in regions of strong topography, notably in the vicinity of Drake Passage, to the south of New Zealand (near the Campbell plateau), and the area to the southeast of Africa (near the Crozet and Ker-

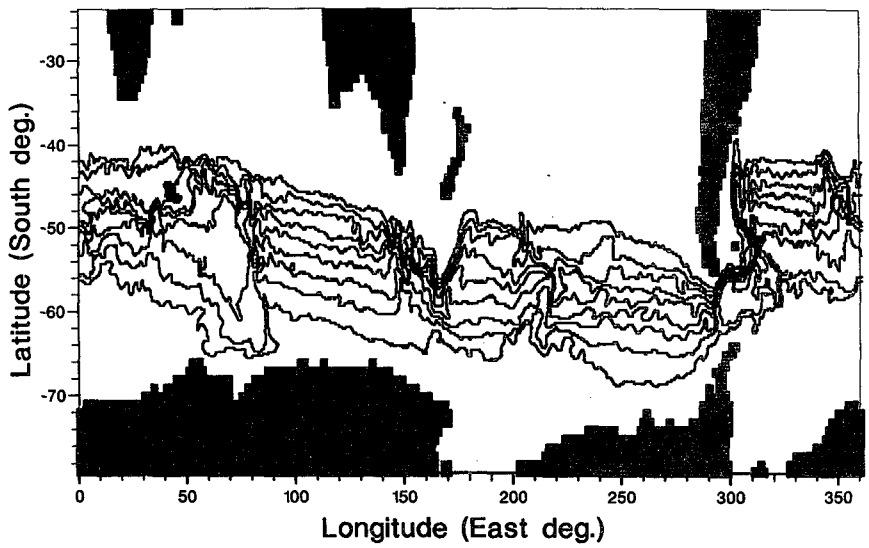

FIG. 1. The time-averaged barotropic streamlines of the ACC from FRAM. These streamlines are used as the alongstream coordinate in this study. The streamlines range from 10 to 170 Sv, with an interval of 10 Sv. The 10-Sv contour is farthest north.

guelen Plateaus). There are regions of strong convergence and divergence of streamlines particularly along the northern flank of the ACC.

We will investigate the integral properties of the ACC along its path by taking the mean barotropic streamfunction to define integration paths. Consider the curvilinear coordinate system (x_1, x_2, z), with velocity components (v_1, v_2, w). Here x_1 is the alongstream coordinate, x_2 is the cross-stream coordinate, and z is the vertical coordinate.

As a definition, an arbitrary field B is separated into a time mean $\bar{B}$ and fluctuation $B^\dagger$ (the transient eddy component). Thus,

$$B = \bar{B} + B^\dagger. \tag{1}$$

The time mean, $\bar{B}$, is further separated into the alongstreamline mean (quasi-zonal mean) $\overline{[B]}$ and departure from this mean, B^* (the so-called standing eddy component), such that

$$\bar{B} = \overline{[B]} + B^*, \tag{2}$$

where

$$\overline{[B]} = \frac{1}{L} \oint_{(\bar{\psi})} \bar{B} dl, \tag{3}$$

L is the length of the streamline, and dl is the differential of the curvilinear path. Note that the standing eddy component will not vanish in the alongstreamline average since we are integrating along the barotropic streamline and the flow field is three-dimensional and sheared in the vertical.

The full field is then given by

$$B = \overline{[B]} + B^* + B^\dagger \tag{4}$$

with the total eddy component (transient and standing)

$$B' = B^* + B^\dagger. \tag{5}$$

Each path is labeled with the total transport in terms of Sverdrups. The flow has a strong barotropic component, and the barotropic streamlines are representative of the direction of the mean flow. It should be borne in mind, however, that there is also a significant baroclinic component to the flow. We will consider streamlines in the range 10 to 170 Sv. The length of individual streamlines gives a measure of the tortuousness of the path. Lengths vary from 33 000 km for the 160-Sv line to 53 000 km for the 50-Sv line. This should be compared to 20 000 km for a line of latitude passing though the Drake Passage at 60°S. Another important property of each streamline for this analysis is the depth of the highest topography along the path. This varies from 790 m for the 10-Sv line to 2279 m for the 80–90 and 150 Sv lines (Fig. 2). This depth is important since the dynamics are very different above and below this level, as shown in section 3.

The time and alongstreamline average of the velocity component tangential to each streamline $[\overline{v_1}]$ is shown in Fig. 3a for the top 17 levels of the model. (Level 17 is at a depth of 1945 m.) We shall refer to this component of velocity as the quasi-zonal velocity. The shape of the velocity component as a function of streamline is approximately constant with depth. There are three peaks, at ψ = 30 Sv, ψ = 80 Sv (mean core), and ψ = 150 Sv. Between the peaks the two minimum values occur on ψ = 40 Sv and ψ = 140 Sv. The velocity is always positive, ranging from 0.15 m s^{-1} at the surface to 0.03 m s^{-1} at depth. The magnitude of the velocity is some two times as large as the corresponding zonally averaged velocity. The vertical profile of the mean velocity on

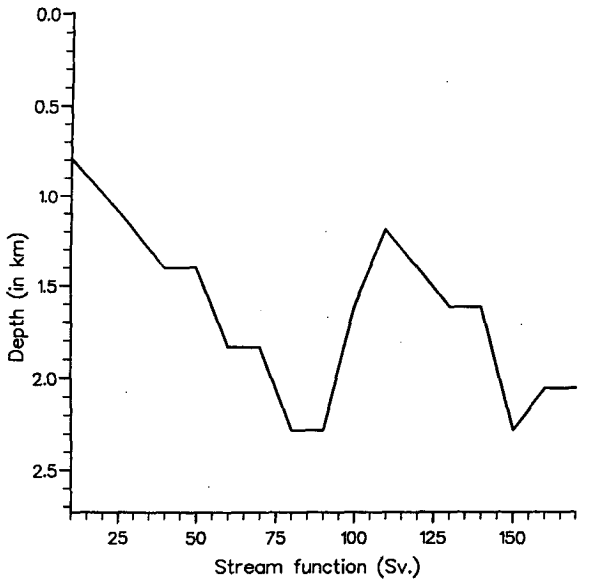

FIG. 2. The depth of the highest topography along a given streamline of the model ACC, as a function of streamline. Flow above this depth is unobstructed.

ψ = 80 Sv is shown in 3b. The depth of the levels of the model are indicated on that figure.

The time- and alongstreamline-averaged normal (or quasi-meridional) velocity component $[\overline{v_2}]$ (disregarding the Ekman layer that is discussed in section 3b) varies considerably with depth (Fig. 4). Between 20 and 790 m there is a small poleward velocity that does not compensate the fairly large (about 10 Sv) equatorward transport in the Ekman layer. Below this depth the normal velocity increases and can become equatorward, especially on the northern flank where topographic features are important. The net mass flux in this lower region is poleward and it balances most of the equatorward flux in the Ekman layer.

The regions of strong ($|\overline{v_2}| > 10^{-2}$ m s^{-1}) quasi-normal velocities along streamlines 20–80 Sv at the 120-m depth are shown in Figs. 5 and 6. The strongest quasi-meridional velocities occur in areas with strong topography: the Drake Passage area, to the south of Australia and New Zealand, and the area to the southeast of Africa. The direction of the cross-ACC flow varies with location. For instance, compare the two northward flowing regions south of New Zealand (where the cross flow is to the right of the ACC) and east of South America (where the cross flow is to the left).

The distribution of the total kinetic energy ($\frac{1}{2}[\overline{u^2 + v^2}]$) in the ACCP looks similar at every level in the upper 2000 m (see Fig. 7). This is indicative of the equivalent barotropic nature of FRAM (Killworth 1992). The highest values occur on the 80-Sv streamline and on the northern flank. In between these two regions there is a local minimum on the 40-Sv streamline. The lowest values occur on the 140-Sv streamline. The highest value is 3.7 $\times$ 10^{-2} m^2 s^{-2}. The total kinetic energy decreases with depth. Figure 8 shows the mean, transient, and standing eddy kinetic energy in the topmost level of the model. At other depths the meridional structure is very similar with the magnitude decreasing with depth as shown in Fig. 7. The eddy kinetic energy is approximately twice that of the mean flow. As with the ACCB, the dominant component of eddy kinetic energy is that of the standing eddies. However, the ratio of transient to standing eddy kinetic energy has increased to around 0.5. Vertical profiles of mean and eddy kinetic energies on the 80-Sv streamline

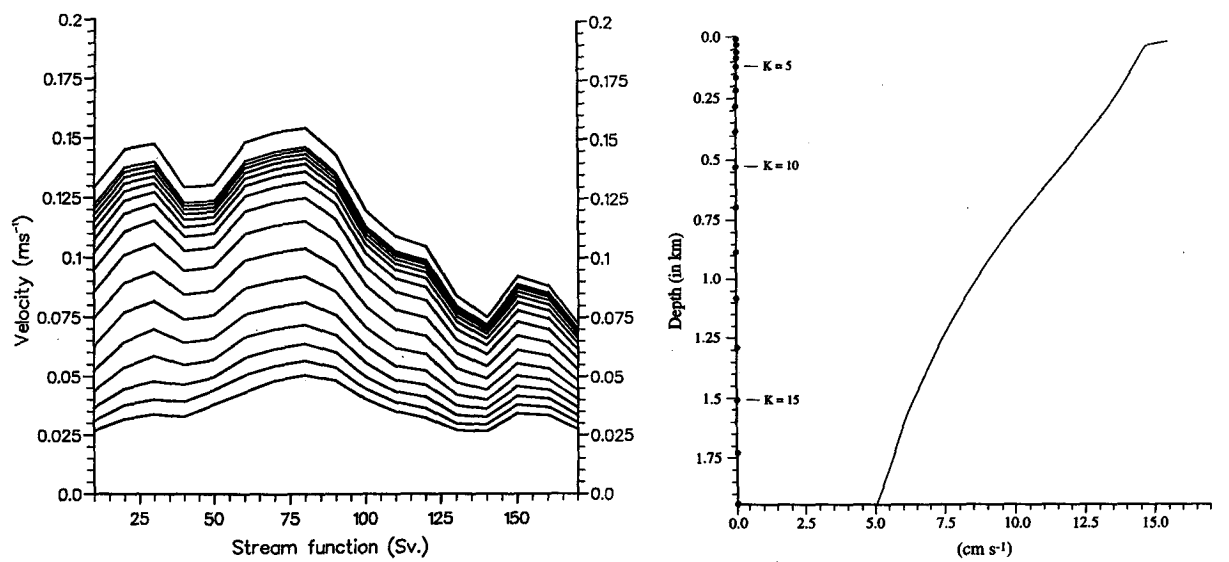

FIG. 3. (a) The alongstreamline average of the alongstreamline component of velocity of the model ACC, for each of the upper 17 model levels as a function of streamline. The current decreases with depth from level 1 (10.15 m) to level 17 (1945 m). (b) Profile of the mean tangential (alongstreamline) velocity at ψ = 80 Sv. The dots on the depth axis correspond to the FRAM levels (from k = 1 to k = 17).

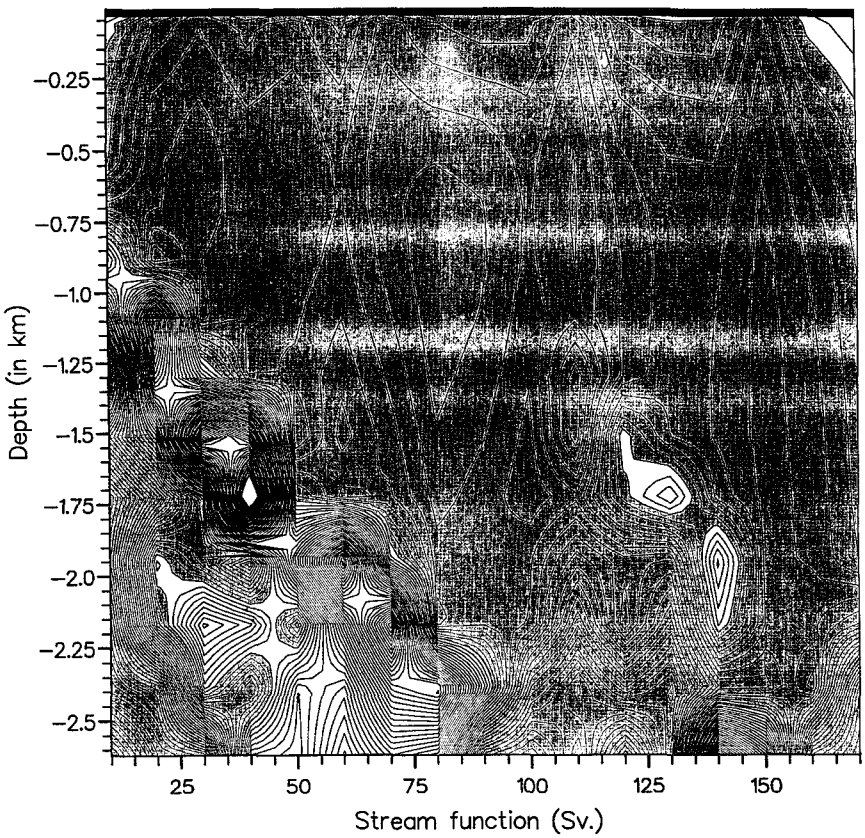

FIG. 4. The alongstreamline average of the cross-stream velocity component of the ACC as a function of depth and streamline. The shaded area represents poleward flow. The contour interval is 9.66 10^{-6} m s^{-1}.

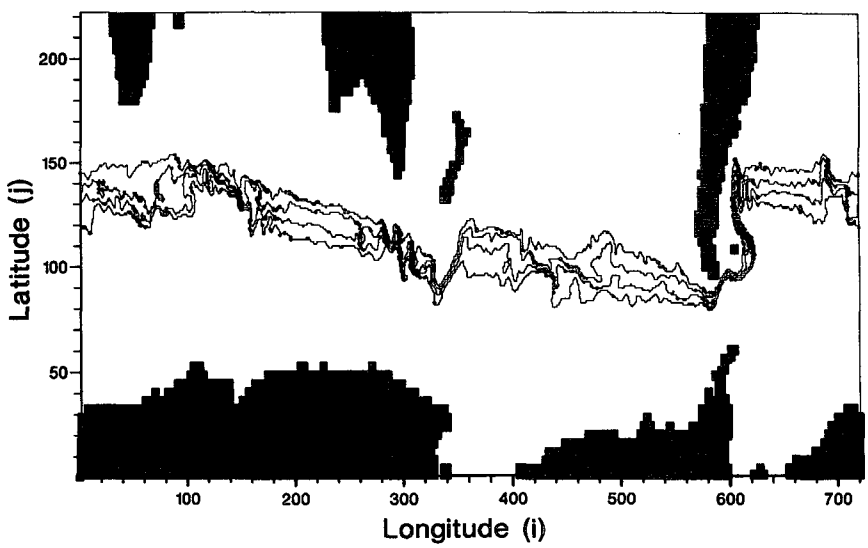

FIG. 5. Regions in which $\overline{v_2} > 10^{-2}$ m s^{-1} at a depth of 120 m along ψ = 20, 40, 60, and 80 Sv, represented by black dots. The (i, j) coordinates correspond to the 0.5° intervals in the zonal direction and 0.25° intervals in the meridional direction.

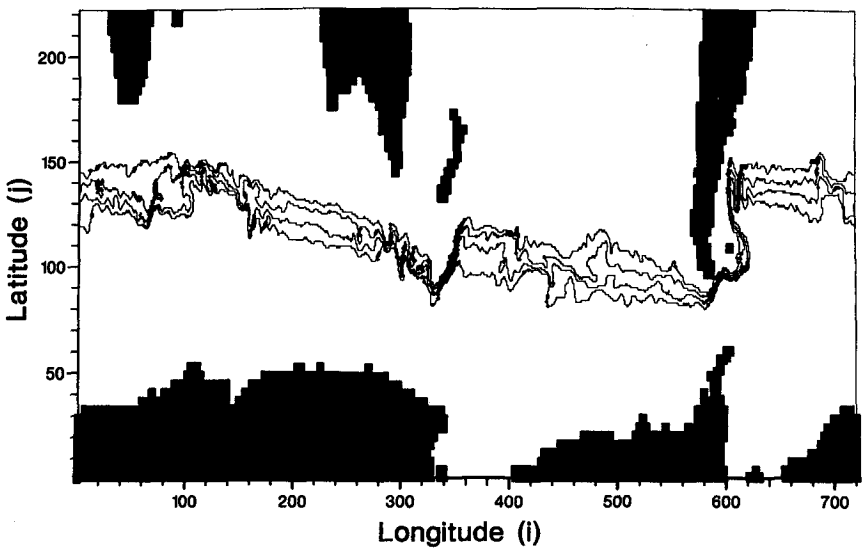

FIG. 6. Regions in which $\overline{v_2} < -10^{-2}$ m s^{-1} at a depth of 120 m along ψ = 20, 40, 60, and 80 Sv. The (i, j) coordinates correspond to the 0.5° intervals in the zonal direction and 0.25° intervals in the meridional direction.

are shown in Fig. 9. The partitioning of energy remains approximately constant with depth. Profiles along other streamlines look similar.

3. The alongstreamline momentum balance

Stevens and Ivchenko (1996) considered the zonal momentum balance of the ACC over the latitudes of Drake Passage (the ACCB). Here we examine the momentum balance along a path, a barotropic streamline, which departs significantly from a line of constant latitude. It is of interest to compare and contrast two balances.

a. The depth-integrated alongstreamline momentum balance

The depth-integrated alongstreamline momentum balance in the curvilinear coordinate system (x_1, x_2, z) can be written as

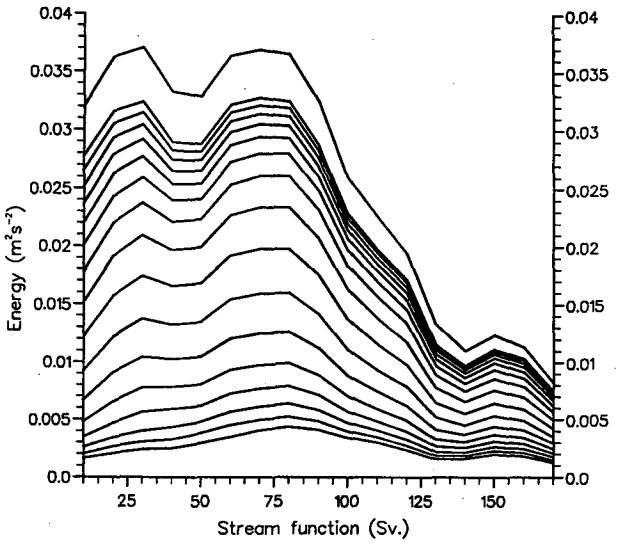

FIG. 7. The alongstreamline average of the total kinetic energy of the model ACC, for each of the upper 17 model levels, as a function of streamline. The energy decreases with depth from level 1 (10.15 m) to level 17 (1945 m).

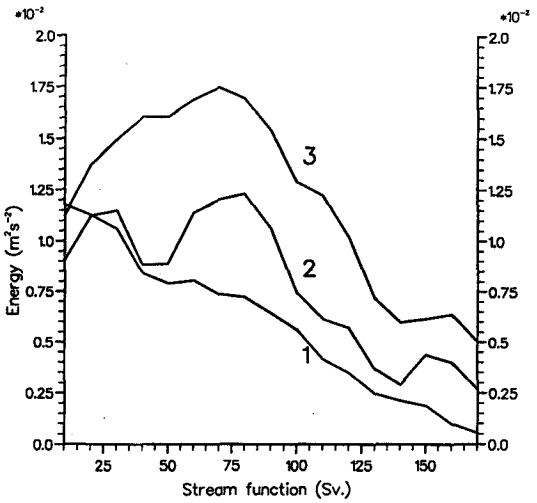

FIG. 8. The alongstreamline average of 1) transient eddy kinetic energy, 2) kinetic energy of the mean flow, and 3) standing eddy kinetic energy for the model level 1 (10.15 m).

$$\overline{\left[\int_{-H}^{0}\left(\frac{\partial v_1}{\partial t}+\frac{1}{h_1h_2}\frac{\partial}{\partial x_1}(h_2v_1^2)+\frac{1}{h_1h_2}\frac{\partial}{\partial x_2}(h_1v_1v_2)+\frac{\partial}{\partial z}(v_1w)-fv_2\right)dz\right]}$$
$$=-\frac{1}{\rho_0}\overline{\left[\frac{1}{h_1}\left(H\frac{\partial p_s}{\partial x_1}+\int_{-H}^{0}\int_{z}^{0}g\frac{\partial\rho}{\partial x_1}dz'dz\right)\right]}+\frac{\overline{[\tau_s^1]}}{\rho_0}-\frac{\overline{[\tau_b^1]}}{\rho_0}+\overline{\left[\int_{-H}^{0}F^{v_1}dz\right]}, \quad (6)$$

where H is the depth, f is the Coriolis parameter, p_s is the surface pressure, ρ is the density, and ρ_0 is a reference density; h_1 and h_2 are the scale factors of the coordinate system. The surface wind stress and bottom friction in the alongstream direction are given by τ_s^1 and τ_b^1, respectively. The horizontal momentum mixing of the alongstream velocity component v_1 is a combination of harmonic and biharmonic terms whose sum is denoted by F^{v_1}.

The study of the zonal balance by Stevens and Ivchenko (1996) found that the wind stress was balanced by the bottom form drag with a small modification from the divergence of Reynolds stress. The balance of terms in (6) computed from the FRAM experiment is shown in Fig. 10 as a function of streamfunction. The wind stress and form drag are still the largest terms in the balance, but other terms are now significant, in particular the horizontal momentum mixing (which is an almost equal combination of harmonic and biharmonic terms) and bottom friction. In the south of the region (160 Sv) the sum of the frictional terms is larger than the form drag. That this is so is not surprising with hindsight. The main jets of ACC are mainly located north of the ACCB (Fig. 1), so the zonal momentum balance is taken over a large region of sluggish water missing much of the dynamics of the ACC. However, the alongstreamline momentum balance follows the main jets, and thus, the horizontal mixing and bottom friction terms are larger, while the magnitude of the wind stress remains the same order of magnitude. As we will see in the following sections, this leads to the northward Ekman flux and the deep southward return current (associated with form drag) having approximately the same magnitude as the purely zonal case. The frictional terms therefore have a greater relative importance.

The horizontal advection of alongstream momentum is equivalent to the divergence of Reynolds stress in the case of a purely zonal analysis. As in the zonal case, this term changes sign across the ACC; thus, it both accelerates and retards the flow. The term remains the same order of magnitude as in the zonal case. The vertical advection of alongstream momentum is larger than in the zonal case and provides a small acceleration to the ACC. The residual term in Fig. 10 consists of the Coriolis term, the unsteady term, and the numerical error. The Coriolis term, which does not occur when considering a purely zonal average, has a negligible effect on the depth-mean balance. The numerical error arises from using the single time level of a model dump [rather then the two time level scheme of Cox (1984)] for calculating the tendencies in Eq. (6). Therefore, it is difficult to separate this term from the unsteady term. Fortunately, their sum is small except on the northward flank of the ACC, $\bar{\psi} \leq 20$ Sv.

The full equation describing the dynamics integrated along a quasi-zonal path and over a depth range h_a to h_b is

$$\overline{\left[\int_{-h_b}^{-h_a}\frac{\partial v_1}{\partial t}dz\right]}+\overline{\left[\int_{-h_b}^{-h_a}\frac{1}{h_1h_2}\frac{\partial}{\partial x_1}(h_2v_1^2)+\frac{1}{h_1h_2}\frac{\partial}{\partial x_2}(h_1v_1v_2)+\frac{\partial}{\partial z}(v_1w)dz\right]}-\overline{\left[\int_{-h_b}^{-h_a}fv_2dz\right]}$$
$$=-\frac{1}{\rho_0}\overline{\left[\frac{1}{h_1}\int_{-h_b}^{-h_a}\frac{\partial p}{\partial x_1}dz\right]}+\overline{\left[\int_{-h_b}^{-h_a}\kappa\frac{\partial^2 v_1}{\partial z^2}dz\right]}+\overline{\left[\int_{-h_b}^{-h_a}F^{v_1}dz\right]}, \quad (7)$$

where p is the pressure and κ is the vertical viscosity. To describe the vertical structure of the momentum balance we will consider three layers.

b. The surface layer

In the directly wind-driven surface layer we find that the wind stress is balanced by a northward Ekman flux (Fig. 11). The major balance in (7) is then

$$-\overline{\left[\int_{-h_{Ek}}^{0}fv_2dz\right]}\approx\frac{\overline{[\tau_s^1]}}{\rho_0}, \quad (8)$$

where h_{Ek} is the thickness of the upper Ekman layer (this is taken to be 20.7 m, the thickness of the upper level of the model). The Ekman velocity is equatorward with magnitude ranging between 0.01 and 0.04 m s^{-1}. All the other terms in this balance are negligible, and their sum is less than 1% of the magnitude of the wind stress and Ekman flux terms.

c. An intermediate layer

In the region below the directly wind-driven layer but above the level of any topographic obstacles ($z = -h_T = 790$ m), the following balance holds

$$\overline{\left[\int_{-h_T}^{-h_{Ek}} \frac{1}{h_1 h_2}\frac{\partial}{\partial x_1}(h_2 v_1^2) + \frac{1}{h_1 h_2}\frac{\partial}{\partial x_2}(h_1 v_1 v_2) + \frac{\partial}{\partial z}(v_1 w)dz\right]} - \overline{\left[\int_{-h_T}^{-h_{Ek}} f v_2 dz\right]} \approx \overline{\left[\int_{-h_T}^{-h_{Ek}} F^{v_1} dz\right]}. \quad (9)$$

This is in contrast to Stevens and Ivchenko (1996), who found that the zonal balance in the region below the wind-driven layer and above topographic obstacles consisted of just two terms: the divergence of Reynolds stress (or poleward momentum flux) and the Coriolis term. The relative size of each term can be seen in Fig. 12. It is worth noting that the magnitude of the terms here are at least an order of magnitude smaller than those in Fig. 10. Thus, it follows that the cross-streamline transport in this layer is an order of magnitude smaller than that in the surface Ekman layer (or in the deep levels where there are topographic obstacles). The horizontal advection of alongstream momentum is almost everywhere positive, which indicates that it provides a net acceleration to the ACC in this region. This is different to the depth-integrated balance and the results of Stevens and Ivchenko (1996) where the divergence of Reynolds stress changes sign. Stevens and Ivchenko (1996) also found that the divergence of Reynolds stress was a net drag on the flow in the intermediate layer. The vertical advection of alongstream momentum provides a net acceleration to the ACC. Again, this is in contrast to the results of Stevens and Ivchenko (1996) who found this term to be small. As one would expect, the horizontal mixing is a drag on the ACC. In the northern flank of the ACC ($\bar{\psi} \leq 100$ Sv) the Coriolis term also provides a drag to the flow. South of the 100-Sv streamline the Coriolis term provides a net acceleration although it does change sign a number of times. The vertical viscosity term of Eq. (7) has a negligible effect; in fact, it is much smaller than the residual. The pressure term of Eq. (7) is also many times smaller than the residual both in the intermediate and surface layers. That this is so is a useful check that the integration along streamlines has been performed correctly.

It is of interest to split the horizontal advection of alongstream momentum into time mean and transient components. The relative sizes of these terms are illustrated in Fig. 13. It can be seen that the contribution from the time-mean flow is entirely positive and thus is accelerating the flow, whereas the transient component is a net drag on the flow. This is a completely different situation to that in predominately zonal flows where the Reynolds stresses due to transients usually accelerate zonal jets (McWilliams et al. 1978).

Integrating zonally within the ACCB Stevens and Ivchenko (1996) found that the contribution of the standing eddies to the eddy momentum flux is very large and dominates the transient eddy component. Integrating along the mean barotropic streamline, the contribution of the standing eddy component is reduced. It is not identically zero because we are integrating along a barotropic streamline and the flow is three-dimensional with a vertical shear.

The Reynolds stress $\overline{[v_1 v_2]}$ and its components (due to mean, transient, and standing eddy motions) at model level 2 (32.5 m) are shown in Fig. 14 as a function of streamfunction. It is positive nearly everywhere, the eddies driving quasi-eastward momentum equatorward. There is little variation in structure with depth (above the level of topographic obstacles). The difference in the Reynolds stress between $\bar{\psi} = 170$ Sv and $\bar{\psi} = 10$ Sv is negative, indicating a net acceleration of the mean flow by the eddies (the pattern does not seem to correspond to the velocity structure). The Reynolds stress is much larger than the normal flux of momentum by the mean flow, $[\overline{v_1}][\overline{v_2}]$ (about an order of magnitude). However, the value of the Reynolds stress is approximately two orders of magnitude too small (and in the wrong direction) to balance the momentum input by the wind. The difference in the transient component between $\bar{\psi} = 170$ Sv and $\bar{\psi} = 10$ Sv is positive, indicating that the transients provide a drag to the ACC (as also noted above). The vertical penetration of momentum is discussed in section 4.

d. A deep layer

At depths greater than 790 m the main marine ridges start to obstruct the ACCP. The balance from this point to the ocean floor is

$$-\overline{\left[\int_{-H}^{-h_T} f v_2 dz\right]} \approx -\frac{1}{\rho_0}\overline{\left[\frac{1}{h_1}\int_{-H}^{-h_T}\frac{\partial p}{\partial x_1}dz\right]} - \frac{\overline{[\tau_b^1]}}{\rho_0} + \overline{\left[\int_{-H}^{-h_T} F^{v_1} dz\right]}. \quad (10)$$

Figure 15 illustrates this balance. There are poleward flowing deep currents associated with pressure differences across the major topographic ridges. This is the topographic form stress. These two terms are dominant

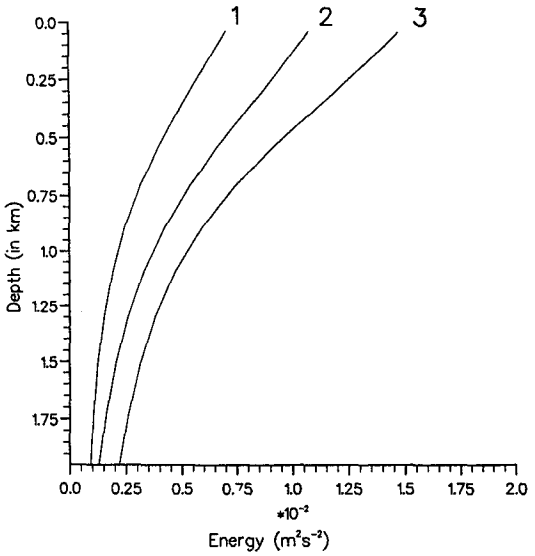

FIG. 9. Vertical profiles of the alongstreamline average of 1) transient eddy kinetic energy, 2) kinetic energy of mean flow, and 3) kinetic energy of the standing eddies on the 80-Sv streamline.

in the balance. However, in contrast to the findings of Stevens and Ivchenko (1996) the other terms are not negligible. In particular, the horizontal mixing of momentum and bottom friction make a contribution. The magnitude of the terms in the balance here is the same order as those in the surface balance of Eq. (8) and Fig. 11.

4. Vertical penetration of momentum

As shown above, the main source of momentum for the ACC in FRAM is the surface wind stress, which is directed predominantly eastward. The principal sink of this momentum is topographic form drag. However this is not the whole story. We need to know how the momentum is transmitted from the surface to the ocean floor where it can be dissipated. The way the stress is transmitted affects the vertical distribution of momentum and hence the transport of the ACC.

The vertical penetration of momentum is achieved through the action of internal (or interfacial) form drag (or stress). Internal form drag occurs in stratified vertically sheared flows with undulating density surfaces, in a similar manner to flow over topography (topographic form drag). Johnson and Bryden (1989) confirmed the importance of internal form drag for a limited region of the ACC, while numerical experiments have shown its importance in both quasigeostrophic (McWilliams et al. 1978; Wolff et al. 1991; Marshall et al. 1993) and primitive equation (Stevens and Ivchenko 1996) models of the Southern Ocean.

The expression for the interfacial form stress can be derived by integrating the momentum equation along a constant density surface. Killworth and Nanneh (1994) directly calculated the distribution of the interfacial form stress for the zonal channel at the Drake Passage latitudes using the FRAM dataset. However, it is possible to derive a proxy term for the interfacial form stress for a depth-coordinate model. Johnson and Bry-

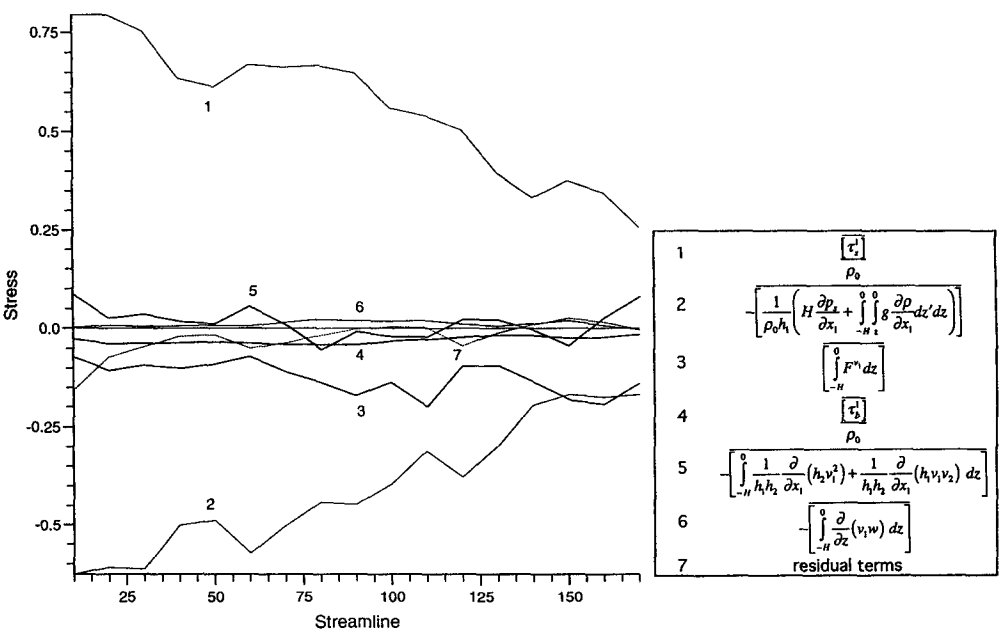

FIG. 10. The depth-integrated, time-, and alongstreamline-averaged momentum balance. Lines 1, 2, 3, 4, 5, 6, and 7 represent the alongstreamline wind stress, bottom form drag, horizontal mixing, bottom friction, horizontal advection of alongstream momentum, vertical advection of alongstream momentum, and remaining (small) terms, respectively. The units are Sv and dynes per square centimeter.

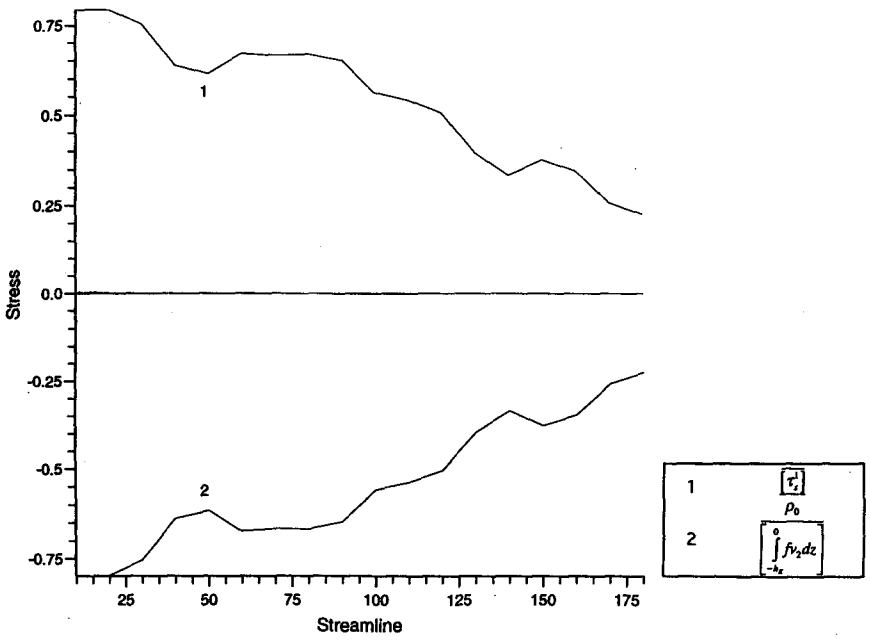

FIG. 11. The time- and alongstreamline-averaged momentum balance in the surface Ekman layer (0–20.7 m). Lines 1 and 2 represent the alongstreamline wind stress and Coriolis terms, respectively. The sum of the remaining small terms is also plotted but is difficult to distinguish from the zero line. The units are Sv and dynes per square centimeter.

den (1989) have shown that because the flow in the open ocean is close to a geostrophic balance, the interfacial form stress could be written in terms of the meridional heat (density) flux, normalized by the vertical temperature (density) gradient. This way of calculating the interfacial form stress is simpler and more appro-

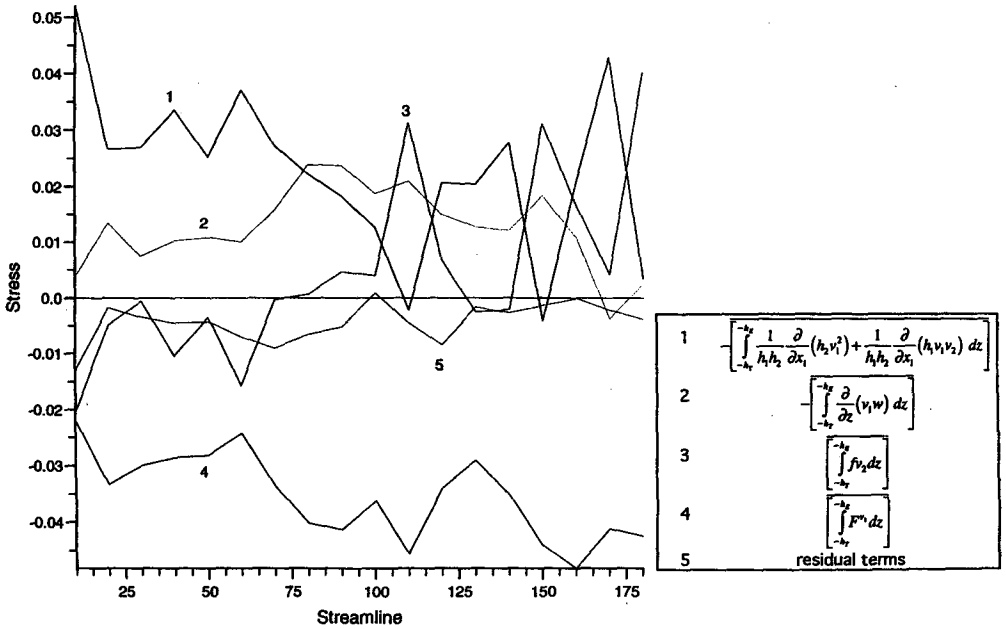

FIG. 12. The time- and alongstreamline-averaged momentum balance at intermediate levels (between levels 2 and 11, 20.7–790 m). Lines 1, 2, 3, 4, and 5 represent the horizontal advection of alongstream momentum, vertical advection of alongstream momentum, Coriolis, horizontal mixing, and remaining (small) terms, respectively. The units are Sv and dynes per square centimeter.

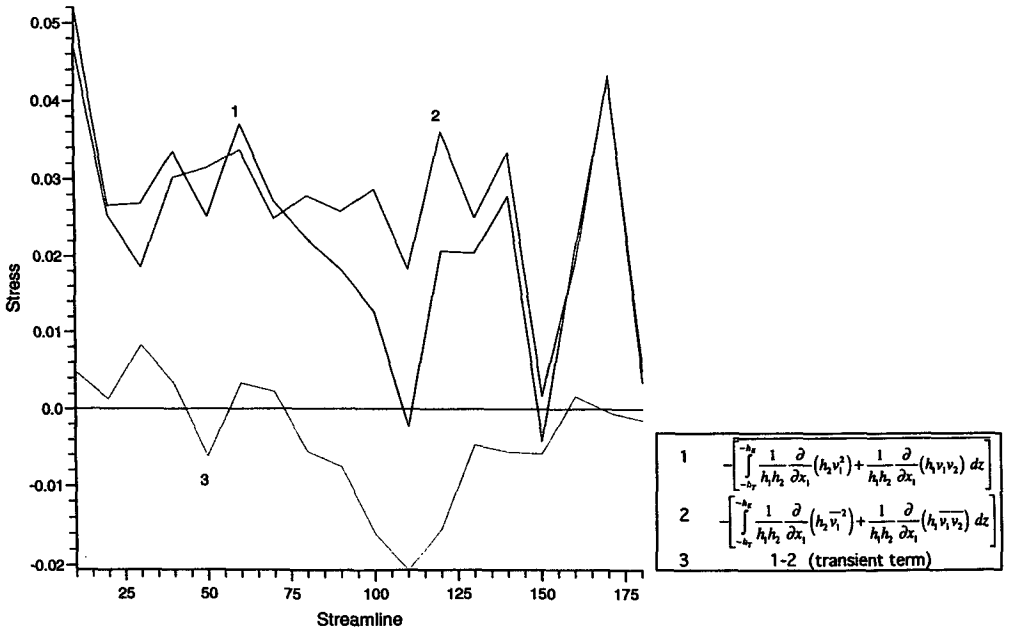

FIG. 13. The time- and alongstreamline-averaged horizontal advection of momentum at intermediate levels (between levels 2 and 11, 20.7–790 m). Lines 1, 2, and 3 represent the total, time mean, and transient components, respectively. The units are Sv and dynes per square centimeter.

priate for the depth-coordinate model used here. We therefore derive an expression for the interfacial form stress by averaging and transforming the continuity and density equations and the expression for the Ekman pumping.

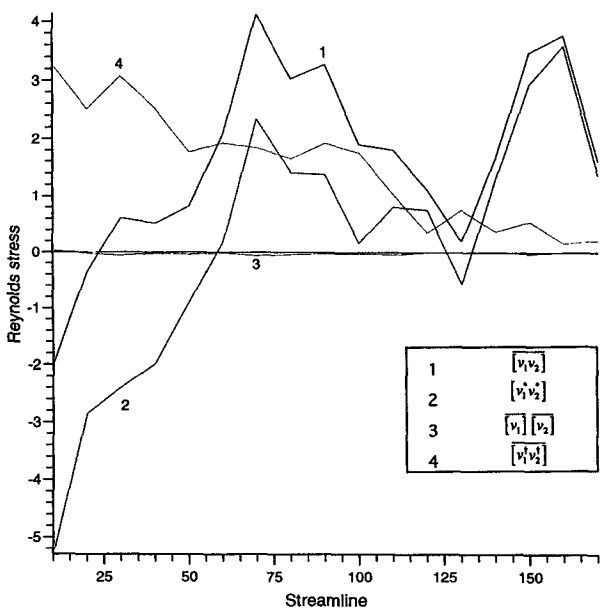

FIG. 14. The alongstreamline-averaged Reynolds stress at model level 2 (32.5 m) and its components. Lines 1, 2, 3, and 4 represent the total, the standing eddy component, the mean component (overturning), and the transient component respectively. The units are Sv and centimeters squared per second squared.

a. General theory

Stevens and Ivchenko (1996) showed that the relationship of Johnson and Bryden (1989) holds (in a quasigeostrophic sense) for a zonal channel with solid meridional boundaries. Stevens and Ivchenko (1996) also showed how the Johnson and Bryden (1989) relationship is modified if the zonal channel has open meridional boundaries allowing a heat flux through the sidewalls. They used the FRAM dataset to confirm their results.

The convoluted path of the ACC raises certain questions about the applicability of the results of Johnson and Bryden (1989) and Stevens and Ivchenko (1996). The analysis of FRAM results by Stevens and Ivchenko (1996) actually missed a good fraction of the total transport. Of particular concern is the reliance on the quasigeostrophic approximation since the stratification and Coriolis parameter both vary significantly along individual streamlines. It is therefore desirable to study the vertical penetration of momentum along the path of the ACC without a quasigeostrophic assumption.

Here we will generalize previous theories to allow integration along an arbitrary path and to include nonquasigeostrophic effects. The result is an expression relating the vertical penetration of alongpath momentum to the wind stress, cross-path density flux, and ageostrophic effects.

We start by integrating the density conservation and continuity equations along the closed path. These equations are then combined by taking the vertical derivative of the density equation and integrating in the cross-path direction from some reference line x_2^0. Finally, we integrate the resultant equation vertically from some depth z to the base of the Ekman layer where the vertical velocity is given by the Ekman pumping induced by the curl of the wind stress. The details are given in appendix A. The result is

$$\rho_0 \frac{[f\overline{\rho' v_2}]}{[\overline{\rho_{(z)}}]}(x_2, z) = \overline{[\tau_s^1]}(x_2) + G(x_2, z) \quad (11)$$

with the function $G(x_2, z)$ given by

$$G(x_2, z) = C(z) + E(x_2, z), \quad (12)$$

where

$$C(z) = \rho_0 \frac{[f\overline{\rho' v_2}]}{[\overline{\rho_{(z)}}]}(x_2^0, z) - \overline{[\tau_s^1]}(x_2^0) + \rho_0 \int_z^{-h_{Ek}} [f\overline{v_2}](x_2^0)dz' \quad (13)$$

and

$$\begin{aligned} E(x_2, z) = &-\rho_0 \int_z^{-h_{Ek}} [f\overline{v_2}](x_2)dz' - \rho_0 \frac{[\overline{\rho}][f\overline{v_2}]}{[\overline{\rho_{(z)}}]}\Bigg|_{x_2^0}^{x_2} + \int_{x_2^0}^{x_2} \frac{1}{L}\frac{\partial L}{\partial x_2'}\overline{[\tau_s^1]}dx_2' \\ &- \rho_0 \int_{x_2^0}^{x_2} \frac{1}{L}\frac{\partial L}{\partial x_2'}\left(\int_z^{-h_{Ek}} [f\overline{v_2}]dz' + \frac{[f\overline{\rho v_2}]}{[\overline{\rho_{(z)}}]}\right)(z)dx_2' - \rho_0 \int_{x_2^0}^{x_2} \frac{[f\overline{\rho v_2}]}{[\overline{\rho_{(z)}}]^2}\frac{\partial}{\partial x_2'}\overline{[\rho_{(z)}]}(z)dx_2' \\ &- \rho_0 \int_{x_2^0}^{x_2} \frac{[fh_2\overline{\rho w_{(z)}}]}{[\overline{\rho_{(z)}}]}(z)dx_2' - \rho_0 \int_{x_2^0}^{x_2} \frac{[fh_2(\bar{w}\rho^*_{(z)} + \overline{w^\dagger \rho^\dagger_{(z)}})]}{[\overline{\rho_{(z)}}]}dx_2'(z) \\ &+ \rho_0 \int_z^{-h_{Ek}} \int_{x_2^0}^{x_2} \left[\frac{h_2}{h_1}\frac{\partial f}{\partial x_1}\overline{v_1}\right]dz'dx_2' + \rho_0 \int_z^{-h_{Ek}} \int_{x_2^0}^{x_2} \left[\frac{\partial f}{\partial x_2'}\overline{v_2}\right]dx_2'dz' + \rho_0 \int_{x_2^0}^{x_2} \frac{\left[\frac{h_2}{h_1}\frac{\partial f}{\partial x_1}\overline{\rho v_1}\right]}{[\overline{\rho_{(z)}}]}(z)dx_2' \\ &+ \rho_0 \int_{x_2^0}^{x_2} \frac{\left[\frac{\partial f}{\partial x_2'}\overline{\rho v_2}\right]}{[\overline{\rho_{(z)}}]}(z)dx_2' + \rho_0 \int_{x_2^0}^{x_2} \frac{[fh_2\bar{Q}]}{[\overline{\rho_{(z)}}]}(z)dx_2', \end{aligned} \quad (14)$$

where Q represents the cross-isopycnal effects. We choose x_2^0 to correspond to the streamline on the southern flank of the ACC. The index in brackets refers to a derivative in the corresponding direction.

The term on the left-hand side of expression (11) describes the proxy term for the interfacial form stress. This is readily shown (Johnson and Bryden 1989) by writing the interfacial form stress as

$$\frac{1}{L}\oint \overline{p\frac{\partial \zeta}{\partial x_1}}dx_1,$$

where ζ is the depth of an isopycnal surface. Integrating by parts using geostrophy and supposing $\zeta = -\rho'/[\bar{\rho}_{(z)}]$ gives us $1/L \oint \overline{p(\partial\zeta/\partial x_1)}\ dx_1 = \rho_0[f\overline{\rho' v_2}]/[\overline{\rho_{(z)}}](x_2, z)$.

b. The functions $G(x_2, z)$, $C(z)$, and $E(x_2, z)$

The expression (11) relates the interfacial form stress averaged along a streamline to the surface stress and the function $G(x_2, z)$. For a zonal channel with closed sidewalls, where the wind stress vanishes and the integration path is taken to be a line of constant latitude then, if quasigeostrophic scaling is applicable, $G(x_2, z) = C(z) = E(x_2, z) = 0$. In this case (11) reduces to the expression given by Johnson and Bryden (1989). That is, the downward flux of eastward momentum is constant with depth, equal to the surface stress, and related to the meridional density flux.

The function $G(x_2, z)$ is nonzero and thus contributes to the momentum penetration when the above assumptions are violated. We have split the function into two parts, $C(z)$ and $E(x_2, z)$.

The function $C(z)$ depends on the density flux, wind stress, and other parameters on the bounding integration path ($x_2 = x_2^0$). We expect the last term in (13) to be small since the flow across streamlines is small. For the $\bar{\psi} = 160$ Sv, this term is at least an order of magnitude smaller than the wind stress. We can interpret $C(z)$ as the influence of the neighboring areas on mo-

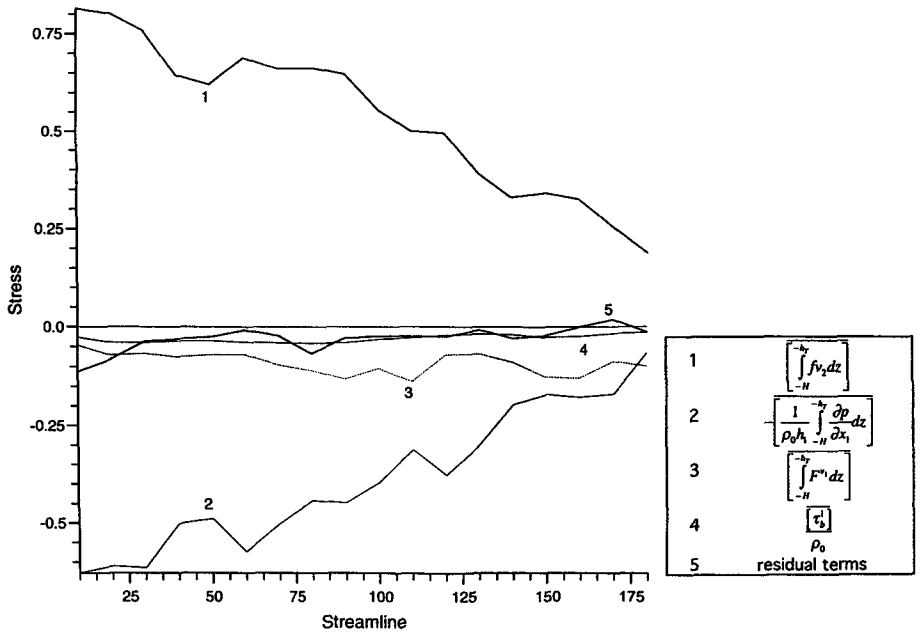

FIG. 15. The time- and alongstreamline-averaged momentum balance at deep levels (between levels 12 and 32, 790–5499 m). Lines 1, 2, 3, 4, and 5 represent the Coriolis, pressure, horizontal momentum mixing, bottom friction, and remaining (small) terms, respectively. The units are Sv and dynes per square centimeter.

mentum penetration within the ACCP. That is, a net quasi-meridional (southward) heat flux through the ACCP requires a vertical (downward) flux of momentum in addition to that induced by the local wind stress. Of course we could take the line x_2^0 to be the coastline of the Antarctic continent in which case the integration constant $C(z)$ would be zero (provided the wind stress is zero along the coast). However, because a net meridional heat transport at a more northerly latitude requires surface outcropping of isopycnic surfaces or diapycnic processes to occur, in order to satisfy the heat budget the effect of the net heat flux would simply be transferred to the function E.

Here E is a function of depth and normal (quasi-meridional) position. The first and second terms on the right-hand side of (14) are proportional to the mean quasi-meridional advection of the planetary vorticity. The third and fourth terms depend on the curvilinear coordinate system and will be small if the path is not too curved [an estimate for the streamlines used in the FRAM dataset is $|L^{-1}(\partial L/\partial x_2)| < 0.1 - 0.4$]. The fifth term depends on the normal variation of the vertical density gradient. The sixth and seventh terms involve the vertical advection of density. Terms 8–11 depend on the variation of the Coriolis parameter along and across the integrated path. The last term in (14) depends upon cross-isopycnic, or diabatic, effects Q. It is difficult to estimate the contributions to Q from the convective regions of the FRAM dataset. Killworth and Nanneh (1994) have shown that for FRAM within the statically stable regions close to the surface, the values of Q are about two orders of magnitude larger than those in the ocean interior; Q increases toward the north, where the convective regime occurs more often. Killworth and Nanneh (1994) suggest that for many purposes Q can be taken as a delta function at the surface.

If it is valid to make a quasigeostrophic approximation, which includes assuming that the horizontal variations in the stratification and Coriolis parameter are small, the integration path is not too curved, and the cross-isopycnal effects are negligible, then $E(x_2, z) \approx 0$ and (11) reduces to the result given by Stevens and Ivchenko (1996). The splitting of G into the two functions, $C(z)$ and $E(x_2, z)$, is rather arbitrary. However, we can use the relative sizes of E and C to give an indication of the importance of non-quasigeostrophic dynamics.

In order to give a physical interpretation to the function $G(x_2, z)$ it is useful to consider two isopycnal surfaces whose heights are given by $\zeta_1(x_1, x_2)$ and $\zeta_2(x_1, x_2)$. For the sake of the argument here we will assume that the departure from the horizontal, $\Delta\zeta_i$, of each surface is small; that is, $\zeta_i = z_i + \Delta\zeta_i$, $|\Delta\zeta_i| \ll |z_i|$, $i = 1, 2$. We will further assume that neither surface outcrops nor intersects topography and that the flow is in a geostrophic balanced state.

Integrating the geostrophic relation between ζ_1 and ζ_2 gives

$$\int_{\zeta_1}^{\zeta_2} f v_2 dz = \frac{1}{\rho_0 h_1} \int_{\zeta_1}^{\zeta_2} \frac{\partial p}{\partial x_1} dz. \qquad (15)$$

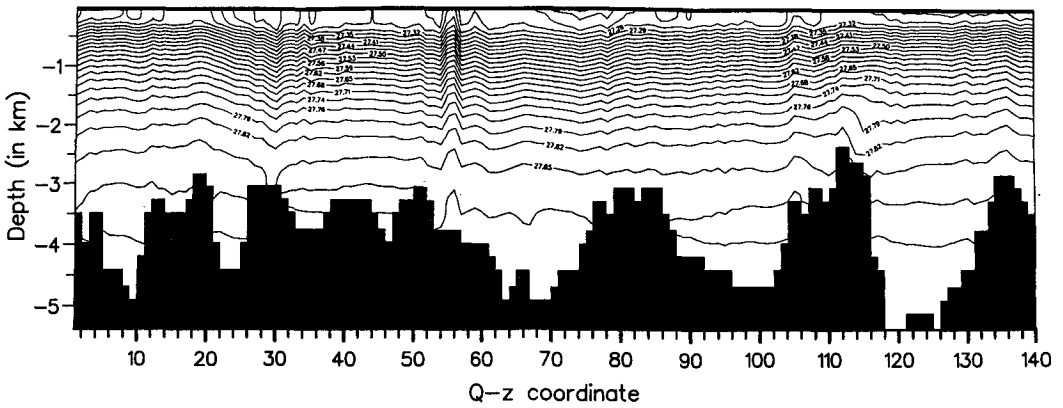

FIG. 16. The density along the 80-Sv streamline as a function of distance along streamline and depth.

Using the relationship

$$p(\zeta_i)\frac{\partial \zeta_i}{\partial x_1} = \frac{\partial p\zeta_i}{\partial x_1} + \rho_0 h_1 f \frac{\rho' v_2}{[\rho_{(z)}]}(x_1, z_i), \quad i = 1, 2 \tag{16}$$

and taking the derivative outside of the integral on the right-hand side of (15) gives

$$\int_{\zeta_1}^{\zeta_2} f v_2 dz = \frac{1}{\rho_0 h_1}\left(\frac{\partial}{\partial x_1}\int_{\zeta_1}^{\zeta_2} p dz - \frac{\partial p\zeta_2}{\partial x_1} - \rho_0 h_1 f \frac{\rho' v_2}{[\rho_{(z)}]} \times (x_1, z_2) + \frac{\partial p\zeta_1}{\partial x_1} + \rho_0 h_1 f \frac{\rho' v_2}{[\rho_{(z)}]}(x_1, z_1)\right). \tag{17}$$

Integrating (17) along the streamlines we obtain

$$\left[\int_{\zeta_1}^{\zeta_2} f v_2 dz\right] = \left[f\frac{\rho' v_2}{[\rho_{(z)}]}\right](z_1) - \left[f\frac{\rho' v_2}{[\rho_{(z)}]}\right](z_2). \tag{18}$$

We assume that

$$\left[\int_{\zeta_1}^{\zeta_2} f v_2 dz\right] = \int_{\zeta_1}^{\zeta_2} [f v_2]_{ip} dz, \tag{19}$$

where $[\ldots]_{ip}$ represents the alongstreamline average along an isopycnal surface. Therefore, using (19) we can rewrite (18) as

$$\int_{\zeta_1}^{\zeta_2} [f v_2]_{ip} dz = -\int_{\zeta_1}^{\zeta_2} \frac{\partial}{\partial z}\left(\frac{[f\rho' v_2]}{[\overline{\rho_{(z)}}]}\right) dz. \tag{20}$$

As ζ_1 and ζ_2 are arbitrary, this can be written as

$$[f v_2]_{ip} = -\frac{\partial}{\partial z}\left(\frac{[f\rho' v_2]}{[\overline{\rho_{(z)}}]}\right). \tag{21}$$

Finally, using (11) we obtain

$$v_{ip} = \frac{[f\overline{v_2}]_{ip}}{[f]} = -\frac{1}{\rho_0[f]}\frac{\partial G}{\partial z}. \tag{22}$$

Thus, the vertical gradient of the function G is proportional to the mean quasi-meridional velocity (along an isopycnal surface).

For a zonal channel with closed sidewalls, where the wind stress vanishes, the integration path is taken to be a line of constant latitude, the quasigeostrophic scaling is applicable, and the source term is small, then $G(x_2, z) = 0$ and $v_{ip} = 0$. If, instead, the sidewalls there are open but quasigeostrophic scaling is still applicable and the source term is small, then $E(x_2, z) = 0$ and

$$v_{ip} = -\frac{1}{\rho_0[f]}\frac{dC}{dz}. \tag{23}$$

In this case v_{ip} is constant with respect to the quasi-meridional coordinate. When E is nonzero this quasi-meridional flow will vary with horizontal position and will imply an effective meridional overturning.

An alternative approach, generalizing Eliassen–Palm fluxes to a curvilinear coordinate system but within a quasigeostrophic framework, is given in the appendix B. There it is shown that the vertical gradient of G is proportional to the residual circulation.

It should be noted that in the FRAM experiment the vertical displacement of the isopycnal surfaces is large and that a large percentage of surfaces outcrop at the surface or cross the bottom relief (Killworth and Nanneh 1994), thus violating the assumptions made in the above analysis. However, following the mean streamfunction there is a substantial depth range over which isopycnal surfaces do not outcrop. Figure 16 shows density plotted with respect to depth and distance along the 80-Sv streamline. Density surfaces between $\sigma = 27.35$ and 27.82 intersect neither the surface nor bottom topography, encompassing the depth range from approximately 500 to more than 2000 m.

c. *Numerical results*

Vertical profiles of

$$I = \rho_0 \frac{[f\overline{\rho' v_2}]}{[\overline{\rho_{(z)}}]}(x_2, z),$$

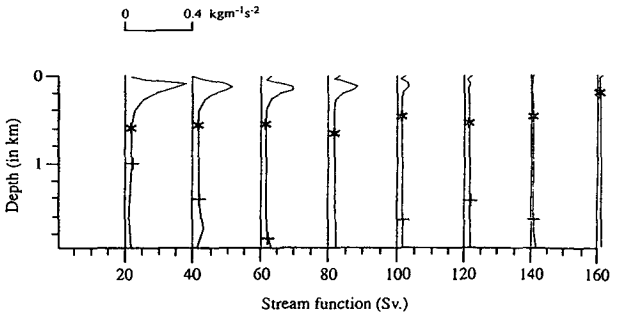

FIG. 17. Profiles of the normalized density flux [the left-hand side of (11)] across the ACC. The marks correspond to the deepest depth of the lightest density surface that never outcrops at the surface (*) and the depth of the highest topography (+) along the streamline.

the time- and alongstreamline-averaged quasi-meridional density flux multiplied by the Coriolis parameter and normalized by the vertical density gradient (interfacial form stress), calculated from the FRAM dataset are shown in Fig. 17 for a number of streamlines. Above 2200 m I is everywhere positive and equivalent to a poleward heat flux. A positive value of I implies a downward penetration of eastward stress by interfacial form stress; I varies both in the horizontal and vertical with values between 0 and 0.34 kg m^{-1} s^{-2}, a similar order of magnitude to the wind stress. There is a general increase in the value of I toward the north.

Within the depth range 500–1500 m the vertical variation of I is small, the major changes being above and below this layer. There is a strong maximum in I between 90 and 160 m, which is greatest on the northern flank of the ACC and disappears toward the south. Below 2200 m I has both positive and negative values.

Also plotted in Fig. 17 are the depths above and below which isopycnal surfaces outcrop or intersect topography, respectively. The region between the two marks show those isopycnic surfaces that do not come into contact with a boundary following the mean streamline. The greatest vertical variation in I occurs where there is direct communication with either the upper or lower boundary. This direct communication can be seen to lead to enhanced vertical penetration of momentum.

The horizontal and vertical variation of I indicates the presence of both a meridional density (heat) flux and nonquasigeostrophic effects. The most striking difference between the analysis along the track of the ACC (ACCP) and that along a line of constant latitude (ACCB) is the maximum in I in the surface layers for the ACCP, which is absent for the ACCB (Stevens and Ivchenko 1996). (The maximum is exaggerated because of the very weak stratification at this depth.) The coincidence of this maximum in I with the maximum depth of isopycnic surface outcropping strongly suggests that the injection of momentum along an outcropping isopycnic surface is a major contribution to the vertical penetration of momentum in the surface

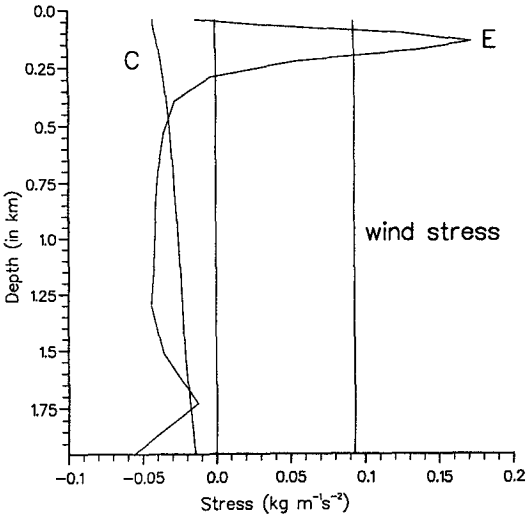

FIG. 18. Profiles of the functions $C(z)$, $E(x_2, z)$, and $[\overline{\tau_s^I}]$ as defined in (11)–(14) for the streamline $\bar{\psi}$ = 40 Sv.

layer (Killworth and Nanneh 1994). Figure 17 also suggests that this direct injection of momentum is greater on the northern flank of the ACC compared with the southern flank where the effect is minimal. The depth to which isopycnic surfaces outcrop in the ACCB is very limited.

The function $C(z)$ has been calculated at $\bar{\psi}$ = 160 and is shown in Figs. 18 and 19. Here $C(z)$ is negative everywhere and increases with depth. Figures 18 and 19 also show the vertical profiles of $E(x_2, z)$, for comparison with $C(z)$, at values of $\bar{\psi}$ = 40 and 140 Sv, respectively. The value of E can then be thought of as giving a measure of the meridional variation of I relative to $\bar{\psi}$ = 160 Sv. At $\bar{\psi}$ = 140 Sv, $|E| \ll |C|$ in the

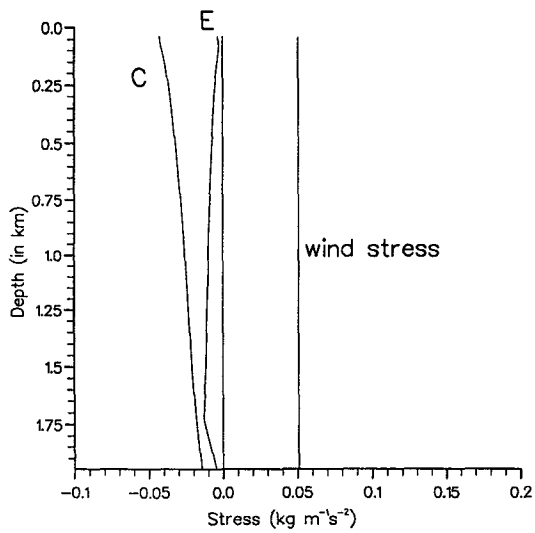

FIG. 19. Profiles of the functions $C(z)$, $E(x_2, z)$, and $[\overline{\tau_z^I}]$ as defined in (11)–(14) for the streamline $\bar{\psi}$ = 140 Sv.

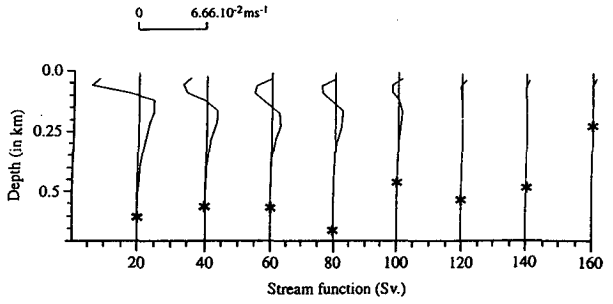

FIG. 20. The isopycnic normal (quasi meridional) velocity as a function of streamline and depth. The mark (*) corresponds to the deepest depth of the lightest density surface that never outcrops at the surface along the streamline.

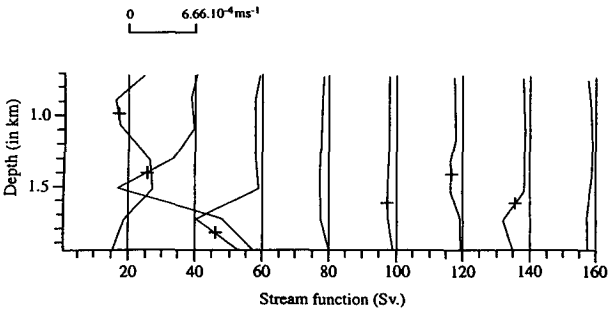

FIG. 21. The isopycnic normal (quasi meridional) velocity as a function of streamline and depth (intermediate layer). The mark (+) corresponds to the depth of the highest topography along the streamline.

upper layers, as one would expect. On the northern flank of the ACC, however, we find that the vertical variation of E usually dominates that of C, indicating the importance of non-quasigeostrophic effects between $\bar{\psi} = 160$ and 40 Sv (and farther north). In particular, the vertical gradient of E in the depth range 500 m to the highest topographic obstacle [the depth range over which (22) applies] is of opposite sign to that of C except toward the bottom of the depth range.

A nonzero value of E has implications for the meridional distribution of the meridional velocity ($E = 0$ implies v_{ip} is constant with $\bar{\psi}$). Figures 20 and 21 show the effective isopycnic quasi-meridional velocity v_{ip} estimated by (22). Attention should be focused on the depth range of no isopycnic outcropping, indicated in the figures, where (22) applies. Usually v_{ip} is negative in this depth range, although toward the northern flank the velocity changes sign. The mean value of v_{ip} averaged over the middepth range between $\bar{\psi} = 40$ and 160 is -5.5×10^{-5} m s^{-1}, with the maximum negative value of the depth-averaged v_{ip}, -8.3×10^{-5} m s^{-1}, occurring on $\bar{\psi} = 120$.

A vertical gradient in the interfacial form stress I, and hence a nonzero value for v_{ip}, implies a tendency to accelerate the quasi-zonal flow. For $v_{ip} < 0$ this acceleration is positive; that is, the vertical transfer of stress is accelerating the flow to the east.

For comparison Fig. 22 shows the averaged quasi-meridional velocity $\overline{[v_2]}$ averaged at constant depth. Because the isopycnal surfaces are reasonably flat in the middepth range, this velocity is similar to v_{ip}, although the mean value is approximately two-thirds of that of v_{ip}.

5. Discussion and conclusions

In discussing the results from the present analysis along the path of the ACC (ACCP) it is instructive to compare them with the results from a purely zonal average (ACCB) (Stevens and Ivchenko 1996). Certain aspects of the two analyses are very similar, such as the cross-stream and vertical distributions of velocity and kinetic energy. As is to be expected, the mean velocities along the ACCP are somewhat higher. Also the relative importance of transient to standing eddies is increased for the ACCP, although the dominance of the later for the ACCP shows the importance of the mean baroclinic flow.

The main momentum balances are quite different in the two cases. The depth-integrated balance in the ACCB shows that the wind stress is balanced almost entirely by topographic form drag, with the remaining terms making little contribution. In the ACCP the lateral friction is an important addition to the topographic form drag (not less than 15%, usually 30%–50%, and at the southern flank of the ACC even larger than the form drag). The reason is because the velocities and their horizontal gradients are much larger in the ACCP than the ACCB. Furthermore, many of the other terms are nonnegligible.

The same reason leads to the big difference in the momentum balances above topographic obstacles. In the ACCB the main balance is between the Reynolds stress divergence and the Coriolis force. In the ACCP the lateral mixing and vertical advection also play an important role in this balance.

A surprising result is the nature of the transient eddy–mean flow interaction along the ACCP. In quasi-

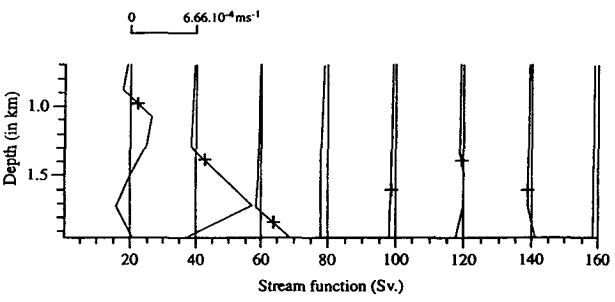

FIG. 22. Vertical profiles of the normal velocity at a fixed level. The mark (+) corresponds to the depth of the highest topography along the streamline.

geostrophic eddy-resolving experiments with a zonal flow, transient eddies are found to accelerate and tighten the mean flow (the "negative viscosity" effect) (e.g., see McWilliams et al. 1978). The same result was found by Stevens and Ivchenko (1996) in the ACCB. In the ACCP, however, with its huge meridional displacements, the total effect by the transient eddies is a dragging effect. There are no theoretical reasons why transient eddies cannot act in either sense. The reason why they should act differently in the ACCB and ACCP is unclear and requires further study.

The background stratification in the Southern Ocean depends strongly on location. Along the barotropic mean streamfunction the stratification in the main thermocline is much greater on the northern flank of the ACC compared to the southern flank, whereas the upper ocean toward the north is very weakly stratified. The importance of the stratification on the dynamics of the ACC comes through in the way stress is transmitted vertically [the $\rho_{(z)}$ term on the lhs of (11)] and hence the meridional structure of the ACC. For the ACCB the stratification is much more uniform across the belt. As a consequence of this, quasigeostrophic scaling can be applied and the function $E(x_2, z) \approx 0$ (Stevens and Ivchenko 1996). For the ACCP, however, E takes on relatively high values, quasigeostrophic theory is no longer valid, and as we shall see below there are consequences for the vertical shear of the current.

We have generalized the expression for the downward penetration of momentum taking into account nonlocal, non-quasigeostrophic, and adiabatic effects. For a zonal channel with closed sidewalls and when quasigeostrophic scaling applies, this expression reduces to that of Johnson and Bryden (1989). In this case the stress penetration occurs locally with the interfacial form stress being constant with depth and equal to the surface wind stress. For the ACC, however, we have found that the net meridional buoyancy flux, changes in stratification, and the surface outcropping of isopycnic surfaces are also important. The results from FRAM show that the wind-driven and thermohaline circulations are intimately linked. In a quasigeostrophic context, this linking can be viewed in terms of a residual meridional circulation (see appendix B).

To highlight the importance for the structure of the ACC of the extra terms of the generalized theory in expression (11), it is interesting to relate the interfacial form stress I [the rhs of (11)] to the vertical shear of the zonal current. Following the argument of Johnson and Bryden (1989), we expect (see appendix C) that

$$\frac{\partial V}{\partial z} \approx \frac{1}{\rho_0} \alpha_0 \overline{[|\rho_{(z)}|]}^{1/2} I^{1/2}, \qquad (24)$$

where $\partial V/\partial z = [(\overline{\partial v_1/\partial z})^2]^{0.5}$—the rms of the vertical gradient of the tangential velocity, averaged along streamline; the coefficient α_0 is given by expression (C7). By fitting the above expression to the results from FRAM at $\bar{\psi} = 20$ Sv, we find $\alpha_0 = 20.8\ \mathrm{m}^{-1/2}$. It is noteworthy that this value of α_0 is within a factor of 2–3 of that used by Johnson and Bryden (1989) when the value they use for the correlation coefficient α_1 is substituted into (C7) together with the alongstreamline averages of f, the Rossby radius L_R, and depth H_0. It should be borne in mind that their value of α_1 was derived from estimates of a rather different regime (see appendix C), and we may not necessarily expect the correlation coefficient to be the same for the present regime. Indeed, we should add the caveat that the relationship (24) uses an eddy parameterization that may not hold everywhere in the very heterogeneous flow conditions existing in the ACC. The utility of (24) is demonstrated by the good comparison with model results given below.

Vertical profiles of the vertical shear, $\partial V/\partial z$, from FRAM and that derived from expression (24) on $\bar{\psi} = 20$ Sv are compared in Fig. 23. The vertical structure of the shear is found to be well represented by (24). Also shown in Fig. 23 is the estimate of shear using the Johnson and Bryden formula [i.e., putting G to zero in (C6)] but using the same value of α_0. Now the vertical structure is very different with a much reduced shear over the top 500 m compared with that below. The physical effects contributing to a nonzero value for G mentioned above are influencing the vertical structure of the zonal current. The action of the negative meridional velocity v_{ip} in accelerating the deep flow is to produce a less sheared, more barotropic flow. The vertical shear has been halved when compared with the purely wind-driven contribution to shear.

Figure 24 shows the vertical shear $\partial V/\partial z$, at $\bar{\psi} = 160$ Sv. Again the estimate from (24) compares well with the actual vertical shear. Here we have used the same value of α_0 as in Fig. 23. Using the alongstream-

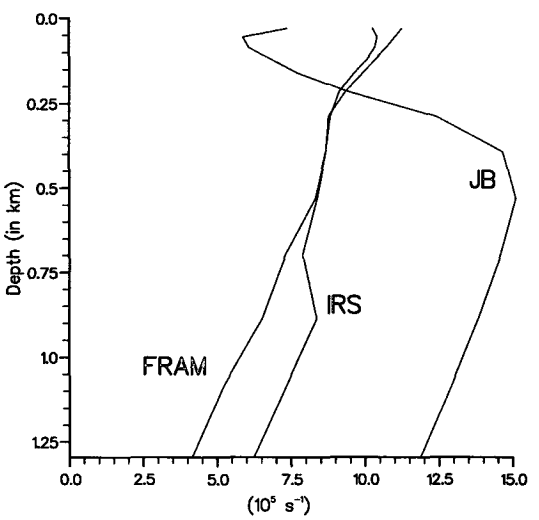

FIG. 23. Vertical profiles of the rms of the vertical gradient of the tangential velocity, $\partial V/\partial z$, (in $10^5\ \mathrm{s}^{-1}$), averaged along $\psi = 20$ Sv calculated using the FRAM dataset and as estimated by the expressions of Johnson and Bryden (1989), and Eq. (C6) (IRS).

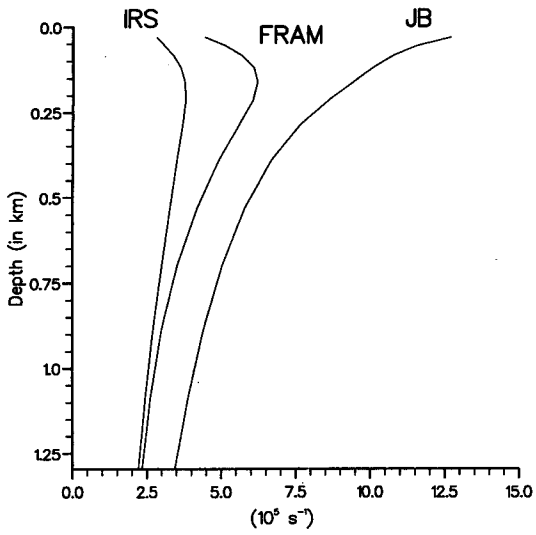

FIG. 24. Vertical profiles of the rms of the vertical gradient of the tangential velocity, $\partial V/\partial z$, (in 10^5 s^{-1}), averaged along $\psi = 160$ Sv calculated using the FRAM dataset and as estimated by the expressions of Johnson and Bryden (1989), and (C6) (IRS).

line averages of f, L_R, and H_0 but keeping α_1 constant, then (C7) would imply that α_0 should increase by 10%, which improves the comparison. Again the Johnson and Bryden estimate has a somewhat different vertical structure, in this case overestimating the near-surface shear.

Analyzing the dynamics of the ACC along its path has produced some interesting and sometimes unexpected results. The analysis shows the incompleteness of purely zonal averaging and the incomplete physics of zonal channel models. There are obvious concerns about the marginal resolution of FRAM, and further studies are needed at higher resolution to properly resolve the mesoscale eddy field and to confirm the numerical results presented here. However, this study does demonstrate the need to analyze the flow along a path approximating the path of the ACC. In our calculations we have chosen to use the time-averaged barotropic streamfunction as the "path of the ACC." That the tangential velocity averaged alongstreamline is much larger (about four orders of magnitude) than the alongstreamline-averaged normal velocity supports our choice. In supplementary calculations we have found that the distribution of properties is quite stable to small variations of the trajectory. Gille (1995) who performed a similar streamwise analysis of the momentum budget of the ACC using the Semtner and Chervin (1992) model, but along contours of sea surface height, found a similar distribution of properties. We therefore suggest that the results we present here are not very sensitive to the precise choice of integration path.

If it is possible to find a contour in which the mean flow is tangential at each point, and if the contour is closed, then this would of course reduce the standing eddy contribution to zero as suggested by Marshall et al. (1993). However, taking such a path does deny the important role of time-independent flow features in moving properties north/south.

Acknowledgments. We gratefully acknowledge the help and support by the FRAM Team in providing the data from the numerical model experiment and, in particular, Dr. D. Webb with whom we had many useful discussions. This work was supported by the NERC under Grants GST/02/407 (KJR, VOI) and GST/02/408 (DPS). We would like to thank an anonymous reviewer for pointing out an error in the original manuscript.

APPENDIX A

The Penetration of Alongstreamline Momentum: General Case

The density conservation equation can be written as

$$\frac{\partial \rho}{\partial t} + \nabla\cdot(\mathbf{v}\rho) = Q, \tag{A1}$$

where Q represents the divergence of cross-isopycnal fluxes. In the curvilinear coordinate system this equation can be written as

$$\frac{\partial \rho}{\partial t} + \frac{1}{h_1 h_2}\left\{\frac{\partial (h_2 \rho v_1)}{\partial x_1} + \frac{\partial (h_1 \rho v_2)}{\partial x_2}\right\} + w\rho_{(z)} + \rho w_{(z)} = Q, \tag{A2}$$

where the index in brackets refers to a derivative in the corresponding direction.

Multiplying (A2) by fh_1h_2, averaging with time and along a closed contour, and dividing by $\overline{[\rho_{(z)}]}$ we obtain

$$[fh_2\bar{w}] = -\frac{\partial}{\partial x_2}\frac{[f\overline{\rho v_2}]}{\overline{[\rho_{(z)}]}} - \frac{[f\overline{\rho v_2}]}{\overline{[\rho_{(z)}]}^2}\frac{\partial}{\partial x_2}\overline{[\rho_{(z)}]} - \frac{[fh_2\overline{\rho w_{(z)}}]}{\overline{[\rho_{(z)}]}} - \frac{1}{L}\frac{\partial L}{\partial x_2}\frac{[f\overline{\rho v_2}]}{\overline{[\rho_{(z)}]}}$$
$$- \frac{[fh_2\overline{w^\dagger \rho^\dagger_{(z)}}]}{\overline{[\rho_{(z)}]}} - \frac{[fh_2\bar{w}\rho^*_{(z)}]}{\overline{[\rho_{(z)}]}} + \frac{\left[\frac{h_2}{h_1}\frac{\partial f}{\partial x_1}\overline{\rho v_1}\right]}{\overline{[\rho_{(z)}]}} + \frac{\left[\frac{\partial f}{\partial x_2}\overline{\rho v_2}\right]}{\overline{[\rho_{(z)}]}} + \frac{[fh_2\bar{Q}]}{\overline{[\rho_{(z)}]}}. \tag{A3}$$

The Ekman pumping at the base of the upper Ekman layer ($z = -h_{Ek}$) is

$$w|_{z=-h_{Ek}} = \frac{1}{f\rho_0}\nabla \times \boldsymbol{\tau}|_z = \frac{1}{f\rho_0}\frac{1}{h_1h_2}\left(\frac{\partial \tau_s^2 h_2}{\partial x_1} - \frac{\partial \tau_s^1 h_1}{\partial x_2}\right). \quad \text{(A4)}$$

Averaging this equation in the same manner as before, we obtain

$$[fh_2\bar{w}]|_{z=-h_{Ek}} = -\frac{1}{\rho_0}\frac{\partial}{\partial x_2}\overline{[\tau_s^1]} - \frac{1}{\rho_0}\overline{[\tau_s^1]}\frac{1}{L}\frac{\partial L}{\partial x_2}. \quad \text{(A5)}$$

Applying (A3) at $z = -h_{Ek}$ using (A5) and integrating in the x_2 direction from x_2^0 (taken here to be the southern flank of the ACC) to x_2, we have

$$\frac{[f\overline{\rho v_2}]}{[\overline{\rho_{(z)}}]}(x_2, -h_{Ek}) = \frac{1}{\rho_0}\overline{[\tau_s^1]}(x_2) + C_1 + D_1(x_2), \quad \text{(A6)}$$

where

$$C_1 = -\frac{1}{\rho_0}\overline{[\tau_s^1]}(x_2^0) + \frac{[f\overline{\rho v_2}]}{[\overline{\rho_{(z)}}]}(x_2^0, -h_{Ek}) = \text{const} \quad \text{(A7)}$$

and

$$D_1(x_2) = -\int_{x_2^0}^{x_2}\frac{[f\overline{\rho v_2}]}{[\overline{\rho_{(z)}}]^2}\frac{\partial}{\partial x_2'}\overline{[\rho_{(z)}]}(-h_{Ek})dx_2' - \int_{x_2^0}^{x_2}\frac{[fh_2\overline{\rho w_{(z)}}]}{[\overline{\rho_{(z)}}]}(-h_{Ek})dx_2' - \int_{x_2^0}^{x_2}\frac{[fh_2\overline{w^\dagger \rho^\dagger_{(z)}}]}{[\overline{\rho_{(z)}}]}(-h_{Ek})dx_2'$$
$$- \int_{x_2^0}^{x_2}\frac{[fh_2\bar{w}\,\rho^*_{(z)}]}{[\overline{\rho_{(z)}}]}(-h_{Ek})dx_2' + \int_{x_2^0}^{x_2}\frac{[fh_2\bar{Q}]}{[\overline{\rho_{(z)}}]}(-h_{Ek})dx_2' + \int_{x_2^0}^{x_2}\frac{1}{L}\frac{\partial L}{\partial x_2'}\left(\frac{1}{\rho_0}\overline{[\tau_s^1]} - \frac{[f\overline{\rho v_2}]}{[\overline{\rho_{(z)}}]}\right)(-h_{Ek})dx_2'$$
$$+ \int_{x_2^0}^{x_2}\frac{\left[\frac{h_2}{h_1}\frac{\partial f}{\partial x_1}\overline{\rho v_1}\right]}{[\overline{\rho_{(z)}}]}(-h_{Ek})dx_2' + \int_{x_2^0}^{x_2}\frac{\left[\frac{\partial f}{\partial x_2'}\overline{\rho v_2}\right]}{[\overline{\rho_{(z)}}]}(-h_{Ek})dx_2'. \quad \text{(A8)}$$

Multiplying the continuity equation by f and averaging gives

$$\frac{\partial}{\partial z}[fh_2\bar{w}] = -\frac{\partial}{\partial x_2}[f\bar{v}_2] - \frac{1}{L}\frac{\partial L}{\partial x_2}[f\bar{v}_2] + \left[\frac{h_2}{h_1}\frac{\partial f}{\partial x_1}\bar{v}_1\right] + \left[\frac{\partial f}{\partial x_2}\bar{v}_2\right]. \quad \text{(A9)}$$

From (A3) and (A9) we obtain

$$\frac{\partial}{\partial z}\frac{[f\overline{\rho v_2}]}{[\overline{\rho_{(z)}}]}(x_2) = [f\bar{v}_2](x_2) - [f\bar{v}_2](x_2^0) + \int_{x_2^0}^{x_2}\frac{1}{L}\frac{\partial L}{\partial x_2'}[f\bar{v}_2]dx_2' + \frac{\partial}{\partial z}\frac{[f\overline{\rho v_2}]}{[\overline{\rho_{(z)}}]}(x_2^0)$$
$$- \frac{\partial}{\partial z}\int_{x_2^0}^{x_2}\frac{[f\overline{\rho v_2}]}{[\overline{\rho_{(z)}}]^2}\frac{\partial}{\partial x_2'}\overline{[\rho_{(z)}]}dx_2' - \frac{\partial}{\partial z}\int_{x_2^0}^{x_2}\frac{[fh_2\overline{\rho w_{(z)}}]}{[\overline{\rho_{(z)}}]}dx_2' - \frac{\partial}{\partial z}\int_{x_2^0}^{x_2}\frac{[fh_2\overline{w^\dagger \rho^\dagger_{(z)}}]}{[\overline{\rho_{(z)}}]}dx_2' - \frac{\partial}{\partial z}\int_{x_2^0}^{x_2}\frac{[fh_2\bar{w}\,\rho^*_{(z)}]}{[\overline{\rho_{(z)}}]}dx_2'$$
$$- \frac{\partial}{\partial z}\int_{x_2^0}^{x_2}\frac{1}{L}\frac{\partial L}{\partial x_2'}\frac{[f\overline{\rho v_2}]}{[\overline{\rho_{(z)}}]}dx_2' - \int_{x_2^0}^{x_2}\left[\frac{h_2}{h_1}\frac{\partial f}{\partial x_1}\bar{v}_1\right]dx_2' - \int_{x_2^0}^{x_2}\left[\frac{\partial f}{\partial x_2'}\bar{v}_2\right]dx_2'$$
$$+ \frac{\partial}{\partial z}\int_{x_2^0}^{x_2}\frac{\left[\frac{h_2}{h_1}\frac{\partial f}{\partial x_1}\overline{\rho v_1}\right]}{[\overline{\rho_{(z)}}]}dx_2' + \frac{\partial}{\partial z}\int_{x_2^0}^{x_2}\frac{\left[\frac{\partial f}{\partial x_2'}\overline{\rho v_2}\right]}{[\overline{\rho_{(z)}}]}dx_2' + \frac{\partial}{\partial z}\int_{x_2^0}^{x_2}\frac{[fh_2\bar{Q}]}{[\overline{\rho_{(z)}}]}dx_2'. \quad \text{(A10)}$$

Finally, integrating (A10) with respect to z and using (A6) gives

$$\rho_0\frac{[f\overline{\rho' v_2}]}{[\overline{\rho_{(z)}}]}(x_2, z) = \overline{[\tau_s^1]}(x_2) + G(x_2, z), \quad \text{(A11)}$$

where $G(x_2, z)$ is given by (12).

APPENDIX B

Eliassen–Palm Fluxes in a Curvilinear Coordinate System: A Quasigeostrophic Approach

We shall derive the equation for the Eliassen–Palm fluxes in a curvilinear coordinate system. Such an approach has been found useful in interpreting the total effect of eddying motions on the zonal mean flow of the atmosphere (Eliassen and Palm 1961; Andrews and McIntyre 1976; Edmon et al. 1980). The results derived here can be used for cases in which the mean flow deviates from being purely zonal. We will use the methodology to give a physical interpretation of the result (11) obtained by integrating along the path of the ACC.

As other authors have found, the physical interpretation of the Eliassen–Palm fluxes is easiest done by making a quasigeostrophic approximation; we shall do so here. In particular, we assume that the background

stratification ρ_s depends only on the vertical coordinate z. Moreover, we assume that the Coriolis parameter f does not change significantly along the path of integration. Neither assumption holds for the FRAM dataset. However, again we hope this does not significantly affect the interpretation.

As before, we will work in the curvilinear coordinate system (x_1, x_2, z) with velocity components (v_1, v_2, w). Making the quasigeostrophic assumption the equation for density (A2) becomes

$$\frac{\partial}{\partial t}\rho + \frac{1}{h_1 h_2}\left(\frac{\partial h_2 \rho v_1}{\partial x_1} + \frac{\partial h_1 \rho v_2}{\partial x_2}\right) + w\rho_{s(z)} = 0. \quad \text{(B1)}$$

The equation of motion may be written as

$$\frac{\partial \mathbf{v}}{\partial t} + (\mathbf{v}\cdot\nabla)\mathbf{v} + f\mathbf{k}\times\mathbf{v} = -\frac{1}{\rho_0}\nabla p + \mathbf{D}, \quad \text{(B2)}$$

where $\mathbf{k}$ is the unit vector in the vertical direction and $\mathbf{D}$ represents dissipation. Projecting (B2) onto x_1 gives

$$\frac{\partial v_1}{\partial t} + \frac{1}{h_1 h_2}\left(\frac{\partial h_2 v_1^2}{\partial x_1} + \frac{\partial h_1 v_1 v_2}{\partial x_2} + \frac{\partial h_1 h_2 v_1 w}{\partial z}\right) - fv_2 = -\frac{1}{\rho_0 h_1}\frac{\partial p}{\partial x_1} + D_1. \quad \text{(B3)}$$

Averaging along a streamline we can obtain

$$\frac{\partial}{\partial t}[v_1] + \frac{1}{[h_2]}\frac{\partial}{\partial x_2}\left([h_2]\left[\frac{v_1 v_2}{h_2}\right]\right) - f[v_2] + \delta_u = 0, \quad \text{(B4)}$$

where

$$\delta_u = \left[\frac{1}{h_1 h_2}\frac{\partial h_2}{\partial x_1}v_1^2\right] + \frac{1}{L}\frac{\partial L}{\partial x_2}\left[\frac{v_1 v_2}{h_2}\right] - \frac{1}{[h_2]}\frac{\partial [h_2]}{\partial x_2}\left[\frac{v_1 v_2}{h_2}\right] + \left[\frac{1}{h_2^2}\frac{\partial h_2}{\partial x_2}v_1 v_2\right] + \frac{\partial}{\partial z}[v_1 w] - [D_1]. \quad \text{(B5)}$$

The term δ_u depends upon the curvilinear coordinate system, the vertical advection of the alongstreamline momentum, and dissipation. The fifth and sixth terms on the right-hand side of (B5) can be ignored through the quasigeostrophic approximation and ignoring dissipation. The first four terms will be small provided the integration path is not too convoluted. Thus, we will ignore δ_u.

Following Andrews and McIntyre (1976) and Edmon et al. (1980), we can define the so-called residual circulation as

$$[v_2] = [v_2^r] + \frac{\partial}{\partial z}\left(\frac{[\rho v_2]}{\rho_{s(z)}}\right), \quad \text{(B6)}$$

$$[h_2 w] = [h_2 w^r] - \frac{\partial}{\partial x_2}\frac{[\rho v_2]}{\rho_{s(z)}} - \frac{1}{L}\frac{\partial L}{\partial x_2}\frac{[\rho v_2]}{\rho_{s(z)}}, \quad \text{(B7)}$$

where v_2^r, w^r are the meridional and vertical components of the residual circulation. The third term on the right-hand side of (B7) has been introduced to conserve mass. The equation of motion can then be rewritten as

$$\frac{\partial [v_1]}{\partial t} - f[v_2^r] = \nabla\cdot\mathbf{J}, \quad \text{(B8)}$$

where $\mathbf{J}$ is the Eliassen–Palm (E–P) vector

$$\mathbf{J} = (J_2, J_z), \quad \text{(B9)}$$

with components

$$J_2 = -[h_2]\left[\frac{v_1 v_2}{h_2}\right], \quad \text{(B10)}$$

and

$$J_z = f\frac{[\rho v_2]}{\rho_{s(z)}}. \quad \text{(B11)}$$

The horizontal component J_2 represents the Reynolds stress. The vertical component J_z is proportional to the meridional density flux and connected with the interfacial form stress.

The residual circulation is nondivergent and satisfies the continuity equation

$$\frac{\partial}{\partial x_2}[v_2^r] + \frac{1}{L}\frac{\partial L}{\partial x_2}[v_2^r] + \frac{\partial}{\partial z}[h_2 w^r] = 0. \quad \text{(B12)}$$

The equation for density can be written, using a quasigeostrophic approximation as

$$\frac{\partial}{\partial t}\left(\frac{[h_2\rho]}{\rho_{s(z)}}\right) + [h_2 w^r] = 0. \quad \text{(B13)}$$

Equations (B8), (B12), and (B13) together with the thermal wind equation constitute a complete set of equations in terms of the quantities: 1) the mean alongstreamline velocity, 2) the meridional and the vertical components of the residual circulation, and 3) the density, if we know the E–P vector. The divergence of the E–P vector, therefore, gives the total effect of the eddies (both standing and transient) on the mean flow $[v_1]$ in analogy with the purely zonal case (Edmon et al. 1980). The residual flow arises as a response to the eddy torque on the mean flow.

Differentiating (11) with respect to z, assuming changes in the vertical density gradient and f are small along the integration path, and assuming that, as in the zonally averaged case,

$$|[\overline{v_2}]| \ll \left|\frac{\partial}{\partial z}\frac{[\overline{\rho v_2}]}{\rho_{s(z)}}\right|. \quad \text{(B14)}$$

Then from the time-averaged version of (B6) we find

$$[\overline{v_2'}] \approx -\frac{1}{\rho_0 f}\frac{\partial G}{\partial z}. \quad \text{(B15)}$$

Thus, the function $G(x_2, z)$ [see also Eqs. (12)–(14)] is proportional to the streamfunction for the residual circulation.

APPENDIX C

The Vertical Shear of the Tangential Velocity

Following Johnson and Bryden (1989), we can deduce a relationship between the vertical shear of the alongstreamline current v_1 and the interfacial form stress I. Assuming the eddies are a result of baroclinic instability, then following Green (1970) and Stone (1972, 1974), Johnson and Bryden (1989) suggest that the meridional velocity fluctuations are proportional to the time-mean baroclinic shear of the zonal velocity and that the density fluctuations are proportional to the normal gradient of the time-mean density and the Rossby radius of deformation L_R. In our curvilinear coordinate system we assume the same and write

$$v_2^\dagger \sim H_0 \frac{\partial}{\partial z}\overline{v_1} \quad \text{(C1)}$$

$$\rho^\dagger \sim L_R \frac{1}{h_2}\frac{\partial}{\partial x_2}\overline{\rho}, \quad \text{(C2)}$$

where † refers to transient component [see (1)]. Using the thermal wind equation we then obtain the relation

$$[\overline{\rho^\dagger v_2^\dagger}] = \alpha_1 L_R H_0 \frac{\rho_0 f_0}{g}\left(\frac{\partial V}{\partial z}\right)^2, \quad \text{(C3)}$$

where $\partial V/\partial z = [(\partial\overline{v_1}/\partial z)^2]^{0.5}$—the rms of the vertical gradient of the tangential velocity averaged alongstreamline; α_1 is a correlation coefficient; H_0 and f_0 are the average depth and Coriolis parameter respectively.

For a mean zonal flow it is possible to obtain an analytic estimate for the α_1 under certain circumstances. For example, the theory of Stone (1974) can be used to obtain a value of α_1 appropriate for a particular baroclinically unstable zonal flow. This is the value used by Johnson and Bryden (1989). For the ACC where the path of the mean flow is topographically steered and highly convoluted, both topography and the barotropic shear are likely to be influencing the production of eddy kinetic energy. We prefer to delay the specification of α_1 until later when we compare the results of the analysis with those from FRAM.

The cross-streamline density flux is mainly connected with the transient eddies, at least in the upper 1.5 km (see also Thompson 1993). So, we suggest that $[\overline{\rho^\dagger v_2^\dagger}] = [\overline{\rho' v_2'}]$, where $'$ refers to the total eddy component [see (5)]. To proceed, if we assume the meridional displacement of the flow is not too large, we can write

$$[f\overline{\rho' v_2}] = f_0[\overline{\rho' v_2'}]. \quad \text{(C4)}$$

This approach is not totally applicable to the ACCP because of the correlation between the Coriolis parameter and density fluxes. However, we do not expect the inexactness of (C4) to radically alter the functional relationship we shall derive. Using (C4) we can rewrite Eq. (11) as

$$[\overline{\rho' v_2'}] = \frac{1}{\rho_0 f_0}\overline{[\rho_{(z)}]}([\overline{\tau_s^\dagger}](x_2) + G(x_2, z)). \quad \text{(C5)}$$

From (C3), (C4), and (C5) we obtain

$$\frac{\partial V}{\partial z} = \frac{1}{\rho_0}\alpha_0\sqrt{\overline{[|\rho_{(z)}|]}([\overline{\tau_s^\dagger}](x_2) + G(x_2, z))}, \quad \text{(C6)}$$

where

$$\alpha_0 = \frac{1}{f_0}\left(\frac{g}{\alpha_1 L_R H_0}\right)^{1/2}. \quad \text{(C7)}$$

Equation (C6) relates the vertical shear $\partial V/\partial z$ to the interfacial form stress. Johnson and Bryden (1989) obtain the same result with $G(x_2, z) = 0$. In section 5 we provide an estimate for α_0 by comparing (C7) with data from FRAM. We also show the importance of the term $G(x_2, z)$ for the vertical shear.

REFERENCES

Andrews, D. G., and M. E. McIntyre, 1976: Planetary waves in horizontal and vertical shear: The generalized Eliassen–Palm relation and the mean zonal acceleration. *J. Atmos. Sci.*, **33,** 2031–2048.

Cox, M. D., 1984: A primitive equation, 3-dimensional model of the ocean. GFDL Ocean Group Tech. Rep. No. 1.

Edmon, H. J., B. J. Hoskins, and M. E. McIntyre, 1980: Eliassen–Palm cross sections for the troposphere. *J. Atmos. Sci.*, **37,** 2600–2616.

Eliassen, A., and E. Palm, 1961: On the transfer of energy in stationary mountain waves. *Geophys. Publ.*, **22**(3), 1–23.

The FRAM Group, 1991: Initial results from a fine resolution model of the Southern Ocean. *Eos, Trans. Amer. Geophys. Union,* **72,** 169, 174–175.

Gill, A. E., 1968: A linear model of the Antarctic Circumpolar Current. *J. Fluid Mech.*, **32,** 465–488.

Gille, S. T., 1995: Dynamics of the Antarctic Circumpolar Current: Evidence for topographic effects from altimeter data and numerical model output. Ph.D. thesis, Massachusetts Institute of Technology and Woods Hole Oceanographic Institution, 217 pp.

Gouretski, V., A. Danilov, V. O. Ivchenko, and A. Klepikov, 1987: *Modelling of the Southern Ocean Circulation.* Hydrometeorologisher Publ., Leningrad, 200 pp.

Green, J. S. A., 1970: Transfer properties of the large-scale eddies in the general circulation of the atmosphere. *Quart. J. Roy. Meteor. Soc.*, **96,** 157–185.

Hellerman, S., and M. Rosenstein, 1983: Normal monthly wind stress over the World Ocean with error estimates. *J. Phys. Oceanogr.*, **13,** 1093–1104.

Hidaka, K., and M. Tsuchiya, 1953: On the Antarctic Circumpolar Current. *J. Mar. Res.*, **12,** 214–222.

Ivchenko, V. O., A. M. Treguier, and S. E. Best, 1996: A kinetic energy budget and internal instabilities in the Fine Resolution Antarctic Model. *J. Phys. Oceanogr.*, in press.

Johnson, G. C., and H. L. Bryden, 1989: On the size of the Antarctic Circumpolar Current. *Deep-Sea Res.*, **36,** 39–53.

Killworth, P. D., 1992: An equivalent-barotropic mode in FRAM. *J. Phys. Oceanogr.*, **22,** 1379–1387.

——, and M. M. Nanneh, 1994: Isopycnal momentum budget of the Antarctic Circumpolar Current in the Fine Resolution Antarctic Model. *J. Phys. Oceanogr.*, **24,** 1201–1223.

Krupitsky, A., and M. A. Cane, 1994: On topographic pressure drag in a zonal channel. *J. Mar. Res.*, **52,** 1–23.

Levitus, S., 1982: *Climatological Atlas of the World Ocean.* NOAA Prof. Paper No. 13, U.S. Dept. of Commerce, 173 pp.

Marshall, J., D. Olbers, H. Ross, and D. Wolf-Gladrow, 1993: Potential vorticity constraints on the dynamics and hydrography of the Southern Ocean. *J. Phys. Oceanogr.*, **23,** 465–487.

McWilliams, J. C., and J. S. Chow, 1981: Equilibrium geostrophic turbulence. Part I: A reference solution in a beta plane channel. *J. Phys. Oceanogr.*, **11,** 921–949.

——, W. R. Holland, and J. S. Chow, 1978: A description of numerical Antarctic Circumpolar Currents. *Dyn. Atmos. Oceans,* **2,** 213–291.

Munk, W. H., and E. Palmén, 1951: Note on the dynamics of the Antarctic Circumpolar Current. *Tellus,* **3,** 53–55.

Nowlin, W. D., Jr., and J. M. Klinck, 1986: The physics of the Antarctic Circumpolar Current. *Rev. Geophys.*, **24,** 469–491.

Olbers, D., and C. Wübber, 1991: The role of wind and buoyancy forcing of the Antarctic Circumpolar Current. *Strategies for Future Climate Research,* M. Latif, Ed., Max-Planck-Institute for Meteorology, 161–192.

Rhines, P. B., and W. R. Holland, 1979: A theoretical discussion of eddy-driven mean flows. *Dyn. Atmos. Oceans,* **3,** 289–325.

Semtner, A. J., and R. M. Chervin, 1988: A simulation of the global ocean circulation with resolved eddies. *J. Geophys. Res.*, **93,** 15 502–15 522.

——, and ——, 1992: Ocean general circulation from a global eddy-resolving model. *J. Geophys. Res.*, **97,** 5493–5550.

Stevens, D. P., and P. D. Killworth, 1992: The distribution of kinetic energy in the Southern Ocean: A comparison between observations and an eddy resolving general circulation model. *Philos. Trans. Roy. Soc. London, Ser. B,* **338,** 251–257.

——, and V. D. Ivchenko, 1996: The zonal momentum balance in a realistic eddy resolving general circulation model of the Southern Ocean. *Quart. J. Roy. Meteor. Soc.,* submitted.

Stone, P. H., 1972: A simplified radiative–dynamical model for the static stability of rotary atmospheres. *J. Atmos. Sci.*, **29,** 405–418.

——, 1974: The meridional variation of the eddy heat fluxes by baroclinic waves and their parameterization. *J. Atmos. Sci.,* **31,** 444–456.

Thompson, S. R., 1993: Estimation of the transport of heat in the Southern Ocean using a fine resolution numerical model. *J. Phys. Oceanogr.*, **23,** 2493–2497.

Treguier, A. M., and J. C. McWilliams, 1990: Topographic influences on wind-driven, stratified flow in a β-plane channel: An idealized model for the Antarctic Circumpolar Current. *J. Phys. Oceanogr.*, **20,** 321–343.

Webb, D. J., P. D. Killworth, A. C. Coward, and S. R. Thompson, 1991: *The FRAM Atlas of the Southern Ocean.* Natural Environment Research Council, 67 pp.

Wells, N. C., and B. A. de Cuevas, 1995: Depth-integrated vorticity budget of the Southern Ocean from a general circulation model. *J. Phys. Oceanogr.*, **25,** 2569–2582.

Wolff, J.-O., V. O. Ivchenko, A. Klepikov, and D. Olbers, 1990: The topographic influence on the dynamics of zonal fluxes in the ocean. *Dokl. Acad. Nauk SSSR,* **313,** 970–974.

——, D. Olbers, and E. Maier-Reimer, 1991: Wind-driven flow over topography in a zonal β-plane channel: A quasigeostrophic model of the Antarctic Circumpolar Current. *J. Phys. Oceanogr.*, **21,** 236–264.